JAERI-M
9242

DETAILED ANALYSIS OF THE DYNAMIC BEHAVIOR OF THE JT-60 VACUUM VESSEL UNDER THE SADDLE-LIKE ELECTROMAGNETIC FORCES

December 1980

Hideyuki TAKATSU, Masatsugu SHIMIZU Mitsuru OHTA,
Kanehisa IMAI*, Satoru ONO* and Masakazu MINAMI*

日本原子力研究所
Japan Atomic Energy Research Institute

Detailed Analysis of the Dynamic Behavior of the JT-60 Vacuum Vessel under the Saddle-like Electromagnetic Forces

Hideyuki TAKATSU, Masatsugu SHIMIZU, Mitsuru OHTA,
Kanehisa IMAI*, Satoru ONO* and Masakazu MINAMI*

Division of Large Tokamak Development,
Tokai Research Establishment, JAERI

(Received November 26, 1980)

Dynamic response analyses of the vacuum vessel of JT-60 were carried out under three kinds of saddle-like electromagnetic forces. In the analysis, the dynamic response of the bellows was obtained by dividing it into three components; the first caused by the forced deflection due to the displacement of the adjacent rigid ring, the second caused by the inertia force and the third caused by the saddle-like electromagnetic force.

Eigenvalue analyses showed that the typical rotation mode of the rigid ring around the major radius is found at the 20th with the natural frequency of 46.3 Hz. And from the results of the dynamic response analyses, it was shown that the maximum displacement response of the rigid ring is 3.1 mm and the dynamic response is remarkable in case of plasma disruption with time constant of 1 msec. In cases of start-up and plasma disruption with time constant of 50 msec, the rigid ring vibrates quasi-statically.

Keywords: JT-60 Tokamak Machine, Vacuum Vessel, Dynamic Response, Saddle-like Electromagnetic Force, Bellows, Natural Frequency, Eigenmode

---

* Mitsui Engineering and Shipbuilding Co., Ltd.

JAERI－M 9242

鞍形電磁力に対するＪＴ－６０の真空容器の動的解析

（臨界プラズマ試験装置設計報告・８１）

日本原子力研究所東海研究所大型トカマク開発部
高津　英幸・清水　正亜・太田　充
今井　兼久*・小野　令*・南　真和*

（１９８０年１１月２６日受理）

鞍形電磁力に対するＪＴ－６０の真空容器の動的解析を，プラズマ消滅（消滅時定数１，５０msec）及びプラズマ立ち上げの３ケースについて行った。

ＪＴ－６０の真空容器は，厚肉リングとベローズという剛性及び重量が非常に異る構造物から成る為，動的解析には２つの解析モデルを用いて行い，特に強度的に着目するベローズの応答に関しては，隣接する厚肉リングからの強制変位による準静的応答，隣接する厚肉リングからの強制加振による動的応答及びベローズ自身に作用する鞍形電磁力による動的応答の３成分に分けて求めた。

解析の結果，鞍形電磁力に典型的に対応する厚肉リングの固有振動数は４６.３Hzであり，プラズマ１msec消滅時には，厚肉リングは最大3.1mmの変位を生じ，真空容器の動的挙動が顕著である事がわかった。一方，プラズマ５０msec消滅時や立ち上げ時においては，真空容器の挙動は比較的準静的である事が明らかとなった。

---

*　三井造船（株）

Contents

1. Introduction 1
2. Analysis method 2
   2.1 Analysis method 2
   2.2 Modeling 3
3. Results of dynamic analysis 5
   3.1 Eigenvalue analysis 5
   3.2 Dynamic response analysis 5
4. Conclusion 7
Acknowledgement 8
Nomenclature 8
References 9
Appendix 10

目　　次

1. 序 1
2. 解析手法 2
   2.1 解析手法 2
   2.2 モデル化 3
3. 動的解析結果 5
   3.1 固有値解析 5
   3.2 動的応答解析 5
4. 結　論 7
   謝　辞 8
   記　号 8
   参考文献 9
   付　録 10

1. Introduction

JT-60 is a large tokamak experiment device now under construction at JAERI with the main device parameters of $R = 3.0$ m, $a = 0.95$ m, $B_t = 45$ kG and $I_p = 2.7$ MA. The bird's-eye view is shown in Fig.1.

The vacuum vessel of JT-60 is a high vacuum toroidal chamber located inside the toroidal and poloidal field coils with an egg-shaped cross-section to house the magnetic limiter coils. The vacuum vessel is made by welding together into a torus eight sectorial 65-mm-thick rigid rings and eight parallel 2.5-mm-thick bellows made from Inconel 625. The latter, which has much lower rigidities than the former, is predicted as a weak point of the vacuum vessel from the view point of the mechanical strength [1].

Partial plan view of the vacuum vessel is shown in Fig.2 with its support system. The rigid ring is composed of two 60°-sectors and six 40°-sectors, and supported at the outer side by two support arms extended from the connecting bars. The support columns are connected with each other by connecting bars and supported by the lower support structure.

As the vacuum vessel has a strong electromagnetic interaction with a plasma column, several kinds of eddy currents are induced in the vacuum vessel according to the plasma behavior [2]. And the vacuum vessel is loaded with several kinds of electromagnetic forces caused by the interaction between the eddy currents and the strong magnetic field. Especially, the electromagnetic force due to the interaction between the poloidal component of the eddy current and the toroidal field (hereinafter saddle-like electromagnetic force) is predominant among all. Saddle-like electromagnetic force mainly acts on the rigid ring and rotates it around the major radius and predicted to cause a high stress of the bellows.

These eddy currents have generally shorter time durations (typically from several to milliseconds) compared with the natural period of the vacuum vessel, so the dynamic behavior of the vacuum vessel is of great concern from the view point of the structural design.

In the present paper, the method used in the present analysis and two kinds of computation models are described in Chap.2. And in Chap.3 described are the results of eigenvalue and dynamic response analyses.

2. Analysis method

2.1 Analysis method

As the vacuum vessel is composed of two components having quite different masses and rigidities with each other, it involves a technical difficulty to analyze the detailed dynamic behavior of the whole of the vacuum vessel at a time. Detailed information about the dynamic behavior of the bellows is indispensable for the machine design, because it is predicted as a mechanical weak point of the vacuum vessel. Therefore, in the present analysis, the dynamic response of the vacuum vessel was obtained through three steps of computation using two kinds of computation models. The analysis procedure is shown in Fig.3.

At first, two kinds of finite element models are constructed; one is for the overall analysis named overall model, and the other is for the bellows analysis named bellows model. The details of two computation models are described in Sec.2.2.

Then eigenvalue analysis of each model gives its natural frequencies and eigenmodes. Following the eigenvalue analysis, the overall model is submitted to the dynamic response analysis. In the dynamic response analysis, electromagnetic forces are applied only to the rigid ring and the ports. The kinetic equation of the nodal points are expressed as follows;

$$\begin{bmatrix} M_1 M_2 \\ M_3 M_4 \end{bmatrix} \begin{Bmatrix} \ddot{q}_f \\ \{0\} \end{Bmatrix} + \begin{bmatrix} C_1 C_2 \\ C_3 C_4 \end{bmatrix} \begin{Bmatrix} \dot{q}_f \\ \{0\} \end{Bmatrix} + \begin{bmatrix} K_1 K_2 \\ K_3 K_4 \end{bmatrix} \begin{Bmatrix} q_f \\ \{0\} \end{Bmatrix} = \begin{Bmatrix} Q(t) \\ Q_b(t) \end{Bmatrix} \quad \text{--- (1)}$$

By solving the above equation using modal analysis method, the dynamic responses of the rigid ring, the ports and the support system are obtained.

On the other hand, the dynamic response of the bellows must take forced deflection due to the displacement of the adjacent rigid ring as the electromagnetic forces acting on the bellows into consideration. The displacement vector $\{q_e\}$ of the bellows against the saddle-like electromagnetic force acting on it is obtained by solving the same equation as Eq.(1). And the kinetic equation of the bellows against the forced deflection due to the displacement of the adjacent rigid ring can be written in the following equation.

$$\begin{bmatrix} M_1 M_2 \\ M_3 M_4 \end{bmatrix} \begin{Bmatrix} \ddot{q}_f \\ \ddot{q}_b \end{Bmatrix} + \begin{bmatrix} C_1 C_2 \\ C_3 C_4 \end{bmatrix} \begin{Bmatrix} \dot{q}_f \\ \dot{q}_b \end{Bmatrix} + \begin{bmatrix} K_1 K_2 \\ K_3 K_4 \end{bmatrix} \begin{Bmatrix} q_f \\ q_b \end{Bmatrix} = \begin{Bmatrix} 0 \\ Q_b(t) \end{Bmatrix} \qquad \text{-----} \quad (2)$$

The displacement vector $\{q_f\}$ is divided into two vectors; quasi-static displacement vector $\{q_s\}$ and dynamic displacement vector $\{q_d\}$ against the inertia force acting on the bellows. Considering the balance of forces acting on the free nodal points against the forced displacement of the restrained nodal points $\{q_b\}$, the following equation about $\{q_s\}$ is obtained.

$$\{q_s\} = -[K_1]^{-1}[K_2]\{q_b\} \qquad \text{-----} \quad (3)$$

and developing the Eq.(2), $\{q_d\}$ is expressed in the following equation, providing that the damping term and the inertia force acting on the restrained nodal points are negligibly small.

$$[M_1]\{\ddot{q}_d\} + [C_1]\{\dot{q}_d\} + [K_1]\{q_d\} = [M_1][K_1]^{-1}[K_2]\{\ddot{q}_b\} \qquad \text{-----} \quad (4)$$

$\{q_b\}$ in Eq.(3) and $\{\ddot{q}_b\}$ in Eq.(4) are obtained as the solution of Eq.(1). Therefore, the displacement vector of the bellows $\{q\}$ is expressed as follows;

$$\{q\} = \{q_e\} + \{q_f\} = \{q_e\} + \{q_s\} + \{q_d\} \qquad \text{-----} \quad (5)$$

2.2 Modeling

It is ideal to analyze the whole of the vacuum vessel at a time, but needs too much computation time. Therefore, taking the periodicities of the structure and the saddle-like electromagnetic force, the 60°-sector is selected for the present analysis, because the maximum stress is expected to be observed at the bellows adjacent to the 60°-sectorial rigid ring.

The overall model consists of a 60°-sectorial rigid ring, two adjacent bellows, four bellows supports, four large ports and the support system. The rigid ring is replaced with isotropic shell elements and divided into 24 (in the poroidal direction) × 8 (in the toloidal direction) elements. The bellows is replaced with orthortopic shell elements having the same rigidities as the bellows and divided into 24(p) × 1(t) elements. The relations between stress and strain are expressed in the following equation [3].

$$\begin{Bmatrix} \alpha_x \\ \alpha_y \\ \tau_{xy} \\ M_x \\ M_y \\ M_{xy} \end{Bmatrix} = \begin{bmatrix} D^P_{11} & D^P_{12} & 0 & 0 & 0 & 0 \\ & D^P_{22} & 0 & 0 & 0 & 0 \\ & & D^P_{33} & 0 & 0 & 0 \\ & & & D^B_{11} & D^B_{12} & 0 \\ \text{SYM.} & & & & D^B_{22} & 0 \\ & & & & & D^B_{33} \end{bmatrix} \begin{Bmatrix} \varepsilon_x \\ \varepsilon_y \\ \gamma_{xy} \\ -\partial^2\omega/\partial x^2 \\ -\partial^2\omega/\partial y^2 \\ -\partial^2\omega/\partial x\partial y \end{Bmatrix} \qquad \text{-----} \ (6)$$

, where

$$D^P_{11} = \frac{bt^3}{12I} E/[(1-\nu^2)(1-\frac{b^2t^3\nu^2}{12Ib_w})] \qquad D^B_{11} = \frac{bt^3}{12b_w} E/(1-\nu^2)$$

$$D^P_{12} = \frac{bt}{12I} E\nu/[(1-\nu^2)(1-\frac{b^2t^2\nu^2}{12Ib_w})] \qquad D^B_{12} = \frac{bt^3\nu}{12b_w} E/(1-\nu^2)$$

$$D^P_{22} = \frac{b_wE}{b} / (1-\frac{b^2t^3\nu^2}{12Ib_w}) \qquad D^B_{22} = IE / b(1-\nu^2)$$

$$D^P_{33} = \frac{b}{2b_w} E / (1+ \ ) \qquad D^B_{33} = \frac{b_wt^3}{12b} E / (1+\nu)$$

and σ, τ, M, ε and ω are the normal stress, shearing stress, bending moment, strain and deflection, respectively. And t, b_w and b are the plate thickness, the girth length and the pitch of the bellows and E and ν are the Young's modulus and Poisson's ratio of the bellows material, respectively.

The bellows supports and the ports are replaced with isotropic shell elements and the support system with beam, truss and shell elements. Masses of the various kinds of appendages are also taken into account.

Plan view and elevation of the overall model are shown in Fig.4. The boundaries of the bellows and the connecting bars are given antisymmetric condition.

The bellows model consists of the bellows, a connection ring, an intermediate ring and two bellows supports. The first is replaced with the orthotropic shell elements and divided into 24(p) × 5(t) elements. The second is replaced with isotropic shell elements, the third with beam and the fourth with isotropic shell. The bird's-eye view of the bellows model is shown in Fig.5. And the specifications of two models are summarized in Table 1.

3. Results of dynamic analysis

3.1 Eigenvalue analysis

Eigenvalue analyses of the overall and the bellows models were carried out using the general structural analysis code NASTRAN. The natural frequencies of two models are listed in Table 2 up to the 24th and 12th, respectively.

The 1st natural frequency of the overall model is 10.9 Hz, which is characterized by the horizontal vibration of the rigid ring, as shown in Fig.6. Rotation vibration modes of the rigid ring around the major radius are found in the 8th, the 14th and the 20th eigenmodes, which are shown in Figs.7, 8 and 9, respectively. Especially, the 20th eigenmode with the natural frequency of 46.3 Hz is the typical one corresponding to the motion of the rigid ring under the saddle-like electromagnetic force (Appendix).

The 1st natural frequency of the bellows model is 15.7 Hz and characterized by the expansion and contraction motion of the bellows in its axial direction, as shown in Fig.10. Figures 11, 12 and 13 show the 2nd, the 3rd and the 4th eigenmodes which are the same ones as the 1st eigenmode except that the upper and the lower halves, and the inner and the outer halves are out of phase, respectively.

3.2 Dynamic response analysis

Using the results of the eigenmode analyses, dynamic response analyses were carried out under the load conditions summarized in Table 3. The time behavior and space distribution of the saddle-like electromagnetic forces are based on the eddy currents computed by code

EDDYTORS [4]. Figure 14 shows the time behaviors of the electromagnetic forces acting on the nodal points at the edge of the rigid ring for three cases. That of case 1 is characterized by the inverse saddle-like electromagnetic force, which is a steep rise with the opposite sign to the saddle-like electromagnetic force. Those of case 2 and 3 are the smooth ones compared with that of case 1. The damping coefficient is assumed as 0.5% for all eigenmodes and the solution time step and duration are listed in Table 3.

The dynamic response analyses of the overall model showed that the maximum displacements and stresses of the rigid ring are 3.1, 0.7, 2.1 mm and 8.6, 2.8, 7.8 kg/mm^2 for case 1, 2, 3, respectively. The maximum displacement is observed at the edge of the rigid ring, and the maximum stress at the root of the port.

The displacement revolutions of the edge of the rigid ring (nodes 9, 17, 233 and 241 shown in Fig.4) are shown in Figs.15, 16 and 17 for case 1, 2 and 3, respectively. As the time duration of the saddle-like electromagnetic force is in the vicinity of the natural period of the rotation mode of the rigid for case 1, the dynamic response of the rigid ring is remarkable. On the other hand, in cases 2 and 3, the electromagnetic forces have the time durations much longer than the natural period of the rotation mode of the rigid ring, and the rigid ring vibrates quasi-statically according to the electromagnetic force.

The poloidal distribution of the displacement at the edge of the rigid ring is shown in Fig.18 for case 1 at the time of maximum displacement occurrence. It shows the similar tendency to the static analysis and the maximum displacement of 3.1 mm was observed at the straight section in its poloidal cross-section.

Figures 19 and 20 show the displacement revolutions of the root and the top of the ports for case 1 and 3, respectively. The maximum displacements of the top of the port $(q_X, q_Y, q_Z)_{max}$ are (2.7, 2.4, 4.1) mm, (1.1, 1.0, 0.5) mm and (3.7, 3.1, 1.6) mm for case 1, 2 and 3, respectively. And the top and the root of the port show in-phase displacement revolutions, though the tortional electromagnetic force acts on the port.

The maximum stress of the rigid ring was observed at the root of the port. As is evident from Fig.21, where the outer and the inner surfaces of the rigid ring show the opposite sign, the stress of the rigid ring at the root of the port is mainly due to the bending moment caused by the vibration of the ports.

As mentioned in Chap.2, inertia force acts on the nodal points of the bellows as well as the electromagnetic force. Forces acting on the nodal points 57 and 153 are shown in Figs.22 and 23 for case 1 and 3, respectively. The electromagnetic force is predominant for the load to the nodal point 57, because it is located next to the rigid ring. On the other hand, as the nodal point 153 corresponds to the intermediate ring, electromagnetic force is almost zero and inertia force solely acts on it.

Figures 24, 25 and 26 show the time behaviors of X, Y and Z components of q_s and $q_e + q_d$ of the bellows (nodes 57 and 65, as shown in Fig.5) for case 1, respectively. And Figs.27, 28 and 29 show those for case 2 and Figs.30, 31 and 32 for case 3, respectively. The displacement components $q_e + q_d$ are comparable to q_s in case 1, and on the other hand, in case 3 the former is almost zero and the latter is predominant. This is caused by the fact that the dynamic response of the rigid ring is remarkable in case 1 and the rigid ring vibrates quasi-statically in case 3.

The stress of the bellows is divided into three components σ_s, σ_e and σ_d according to the displacement components q_s, q_e and q_d. Stress revolutions in the elements 26, 122, 31 and 127 of the bellows are shown in Figs.33, 34, 35 and 36 for case 1 and in Figs.37, 38, 39 and 40 for case 3, respectively. The maximums of the stress component σ_s are observed in the element 31, as shown in Figs.35 and 39, and 10.0, 2.6 and 9.8 kg/mm^2 for case 1, 2 and 3, respectively. The maximums of the sum of the stress components σ_e and σ_i are observed in the element 26, as shown in Figs.33 and 37, and 13.2, 3.0 and 1.5 kg/mm^2 for case 1, 2 and 3, respectively. Stress response shows the similar tendency to the displacement response. The maximum stresses are 17.9, 3.9 and 10.3 kg/mm^2 and observed in element 26, 31 and 31 for case 1, 2 and 3, respectively.

4. Conclusion

Dynamic response analyses of the vacuum vessel of JT-60 were carried out under three kinds of saddle-like electromagnetic forces. In the analysis, the dynamic response of the bellows was obtained by dividing it into three components; the first caused by the forced deflection due to the displacement of the adjacent rigid ring, the second caused by the inertia force acting on the bellows and the third caused by the saddle-like electromagnetic force acting on the bellows.

Eigenvalue analyses showed that the typical rotation vibration mode of the rigid ring around the major radius are found at the 20th with the natural frequency of 46.3 Hz. And from the results of the dynamic response analyses, it was shown that the maximum displacement response of the rigid ring is 3.1 mm and the dynamic response is remarkable in case of plasma disruption with time constant of 1 msec, because the time duration of the electromagnetic force is in the vicinity of the natural period of the rotation mode of the rigid ring. On the other hand, in case of start-up and plasma disruption with time constant of 50 msec, the electromagnetic force has the time duration much longer than the natural period of the rotation mode of the rigid ring, and the rigid ring vibrates quasi-statically according to the electromagnetic force.

Structural integrity of the vacuum vessel against three kinds of saddle-like electromagnetic forces was confirmed by the fatigue analyses and to be reported later [5].

Acknowledgement

The authors would like to acknowledge the continuous guidance and encouragement of Drs. Y. Iso, M. Yoshikawa and T. Iijima. They also wish to express their gratitude to the members belonging to the technical committee of ISES 81 group led by Prof. Udoguchi of Chiba University for stimulating and useful discussions and to Mr. Y. Nakamura for computing the eddy currents induced in the vacuum vessel.

Nomenclature

$\{q_f\}$: displacement vector of the free nodal point
$\{q_b\}$: displacement vector of the restrained nodal point
$\{Q(t)\}$: load vector acting on the free nodal point
$[M]$: mass matrix
$[C]$: damping matrix
$[K]$: stiffness matrix

$\{Q_b(t)\}$: reaction force vector of the restrained nodal point

References

[1] TAKATSU, H., SHIMIZU, M., YAMAMOTO, M., OHTA, M.; JAERI-M 8017 (1978).

[2] NINOMIYA, H., NAKAMURA, Y., OZEKI, T., KAMEARI, A., TSUZUKI, N., SOMETANI, T., SUZUKI, Y.; Proc. 8th Symposium on Engineering Problemsof Fusion Research (1979).

[3] MORISHITA, O., TAKATSU, H., TAKASHIMA, T., YAMAMOTO, M., OHTA, M., YOSHII, A., SUZUKI, M.; JAERI-M 6822 (1976).

[4] KAMEARI, A., SUZUKI, Y.; JAERI-M 7120 (1977).

[5] TAKATSU, H., SHIMIZU, M., OHTA, M., UCHINO, K.; to be published.

Appendix

Equation (1) can be expressed as

$$M\ddot{X} + C\dot{X} + KX = Q \qquad \text{--- (A1)}$$

, where

$$M = \begin{bmatrix} M_1 M_2 \\ M_3 M_4 \end{bmatrix}, \quad C = \begin{bmatrix} C_1 C_2 \\ C_3 C_4 \end{bmatrix}, \quad K = \begin{bmatrix} K_1 K_2 \\ K_3 K_4 \end{bmatrix},$$

$$X = \{q_f, \{0\}\}^T, \qquad Q = \{Q(t), Q_b(t)\}^T$$

In the mode superposition analysis, it is assumed that the structural response can be described adequately by the m lowest vibration modes. Using the transformation

$$X = [u]\{\Phi\} \qquad \text{--- (A2)}$$

, where [u] is the normal function and $\{\Phi\}$ is the normal coordinate, Eq.(A1) can be written as

$$\ddot{\phi}_i + 2\zeta_i\omega_i\dot{\phi}_i + \omega_i^2\phi_i = \frac{1}{m_i^*}\{u_i\}^T\{Q(t)\} \qquad \text{--- (A3)}$$

, where

$$m_i^* = \{u_i\}^T[M]\{u_i\}$$

and ζ_i and ω_i are the critical damping coefficient and the angular natural frequency. Under the initial conditions $\dot{\phi}_i(0) = \phi_i(0) = 0$, the solution of Eq.(A3) is expressed in the following equation;

$$\phi_i = \int_0^t \gamma_i \exp\{-\zeta_i\omega_i(t-\tau)\}\sin\omega_{di}(t-\tau)d\tau \qquad \text{--- (A4)}$$

, where

$$\gamma_i = \frac{\{u_i\}^T\{Q\}}{m_i^*\,\omega_{di}}, \qquad \omega_{di} = \frac{\omega_i}{\sqrt{1-\zeta_i^2}} .$$

As is evident from the above equation, the greater γ_i is, the greater is the influence of the ith eigenmode on the dynamic behavior.

γ_i computed for three cases are summarized in Tables A1, A2, A3, A4 and A5 up to the 43th eigenmode, where I is the mode number, and γ_X, γ_Y and γ_Z reveal the X, Y and Z components of γ_i, respectively. As shown in these tables, Z component is the largest among three and the 20th eigenmode shows the maximum, because it has the eigenmode similar to the distribution of the electromagnetic force.

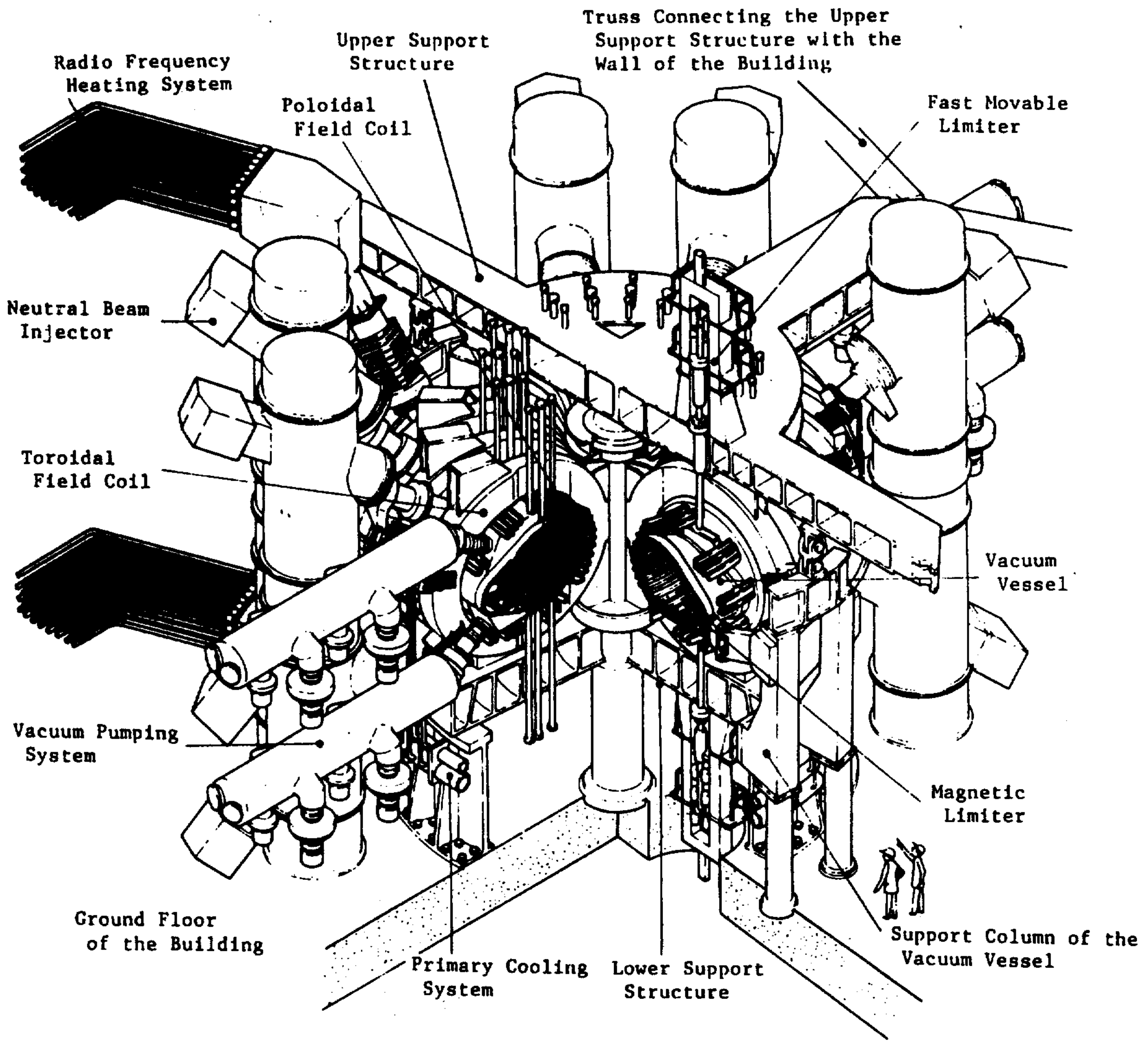

Fig. 1 Bird's-eye view of the tokamak machine of JT-60.

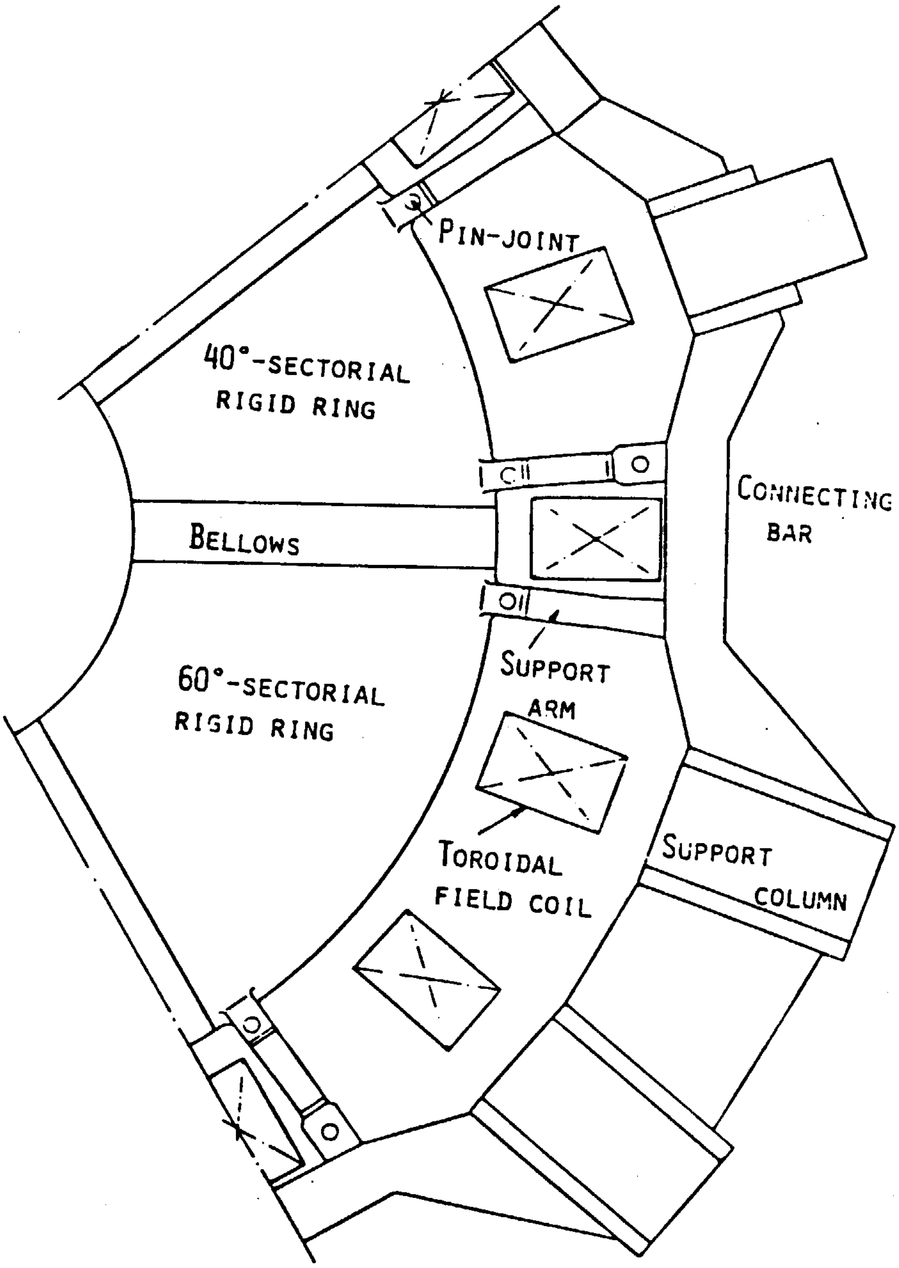

Fig. 2 Partial plan view of the vacuum vessel of JT-60 and its support system.

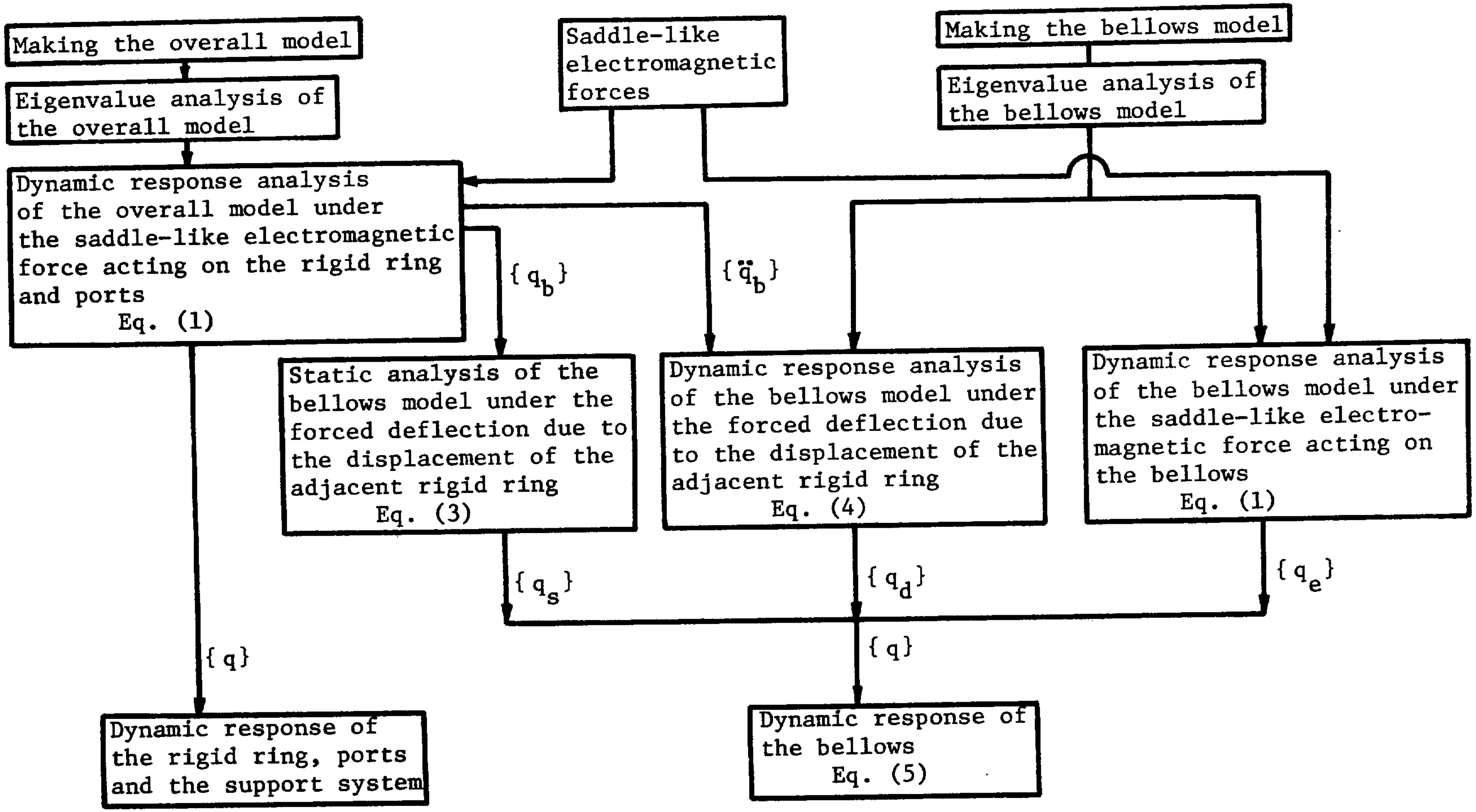

Fig. 3 Analysis procedure.

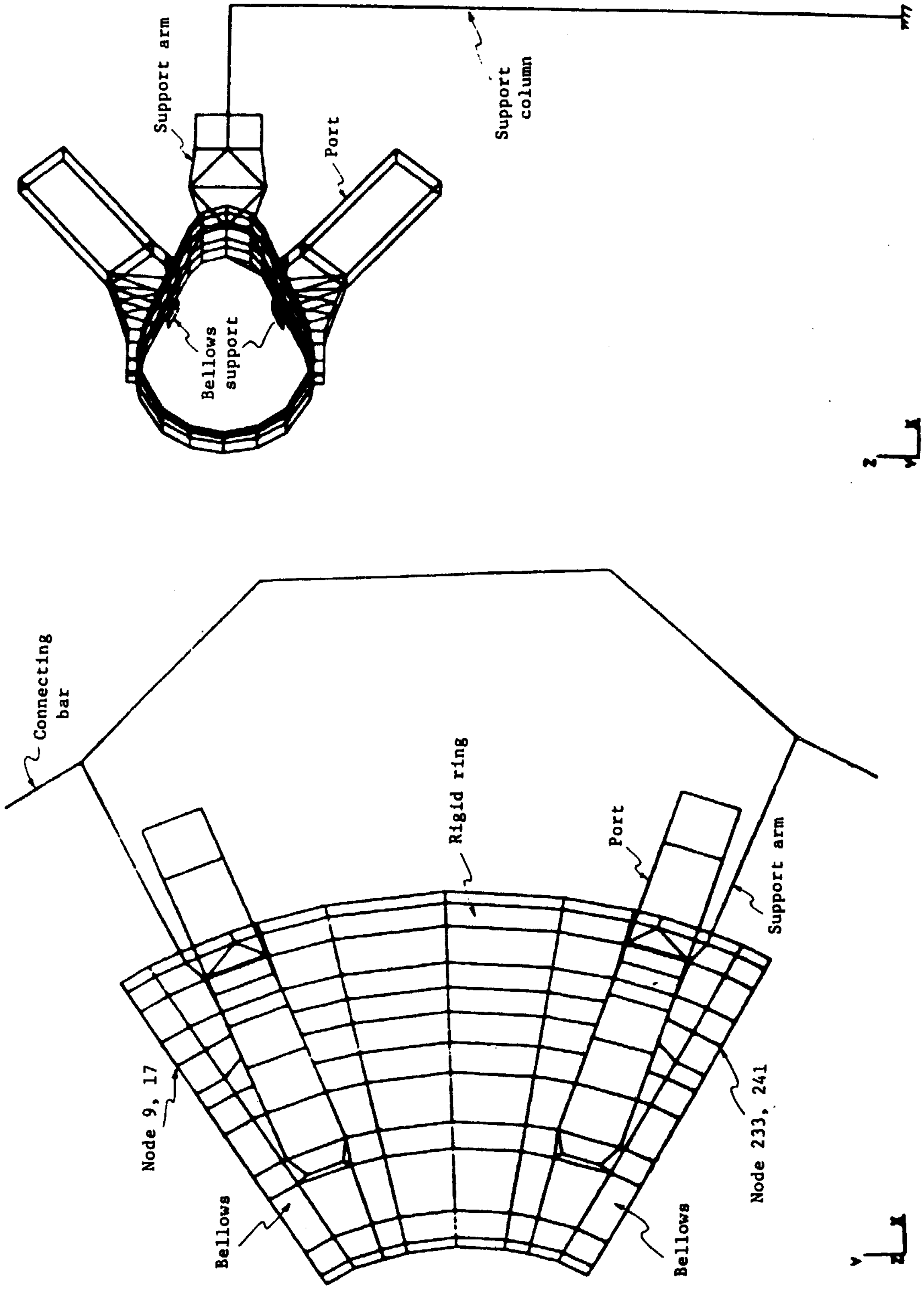

Fig. 4 Plan view and elevation of the overall model.

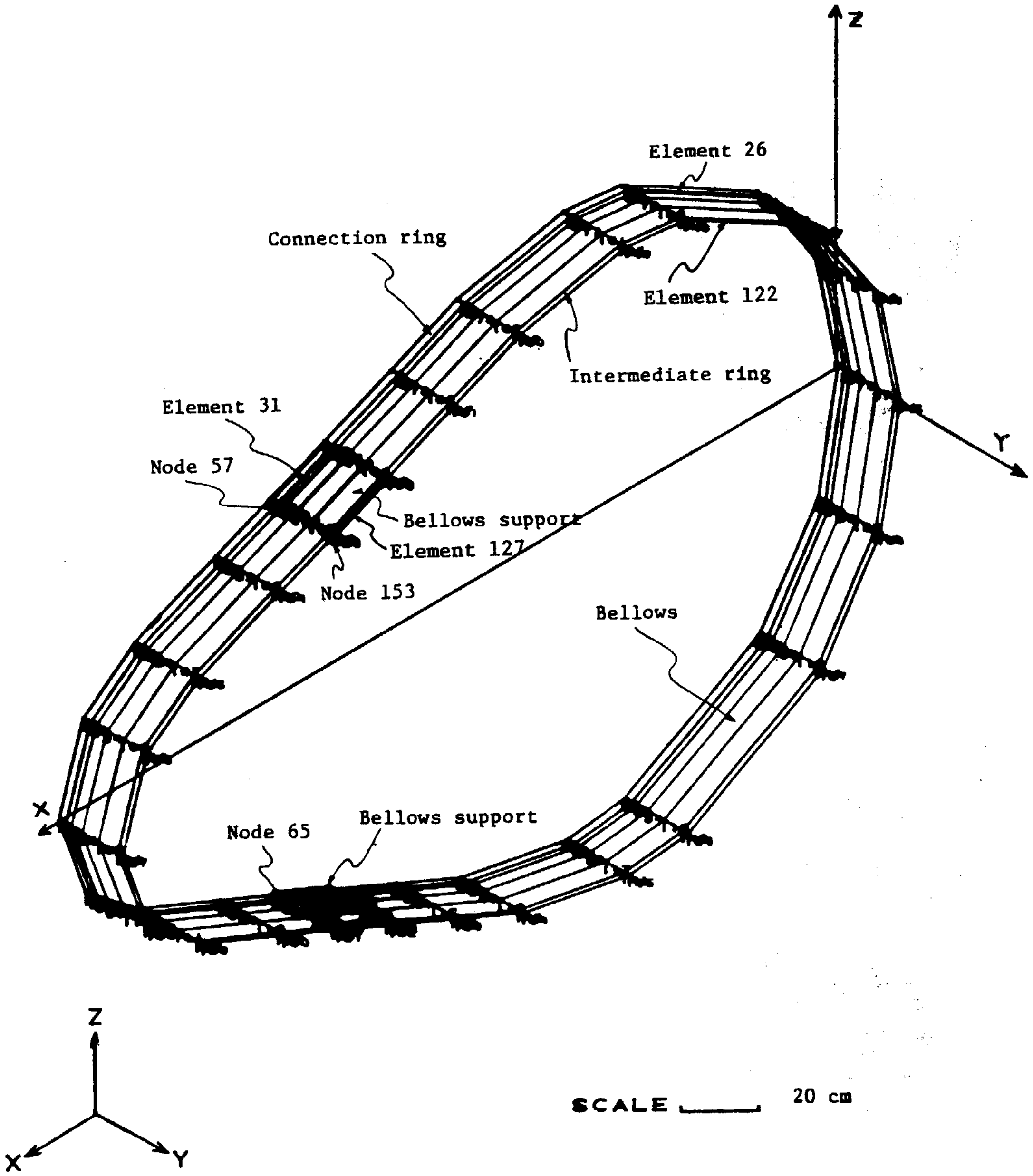

Fig. 5 Bird's-eye view of the bellows model.

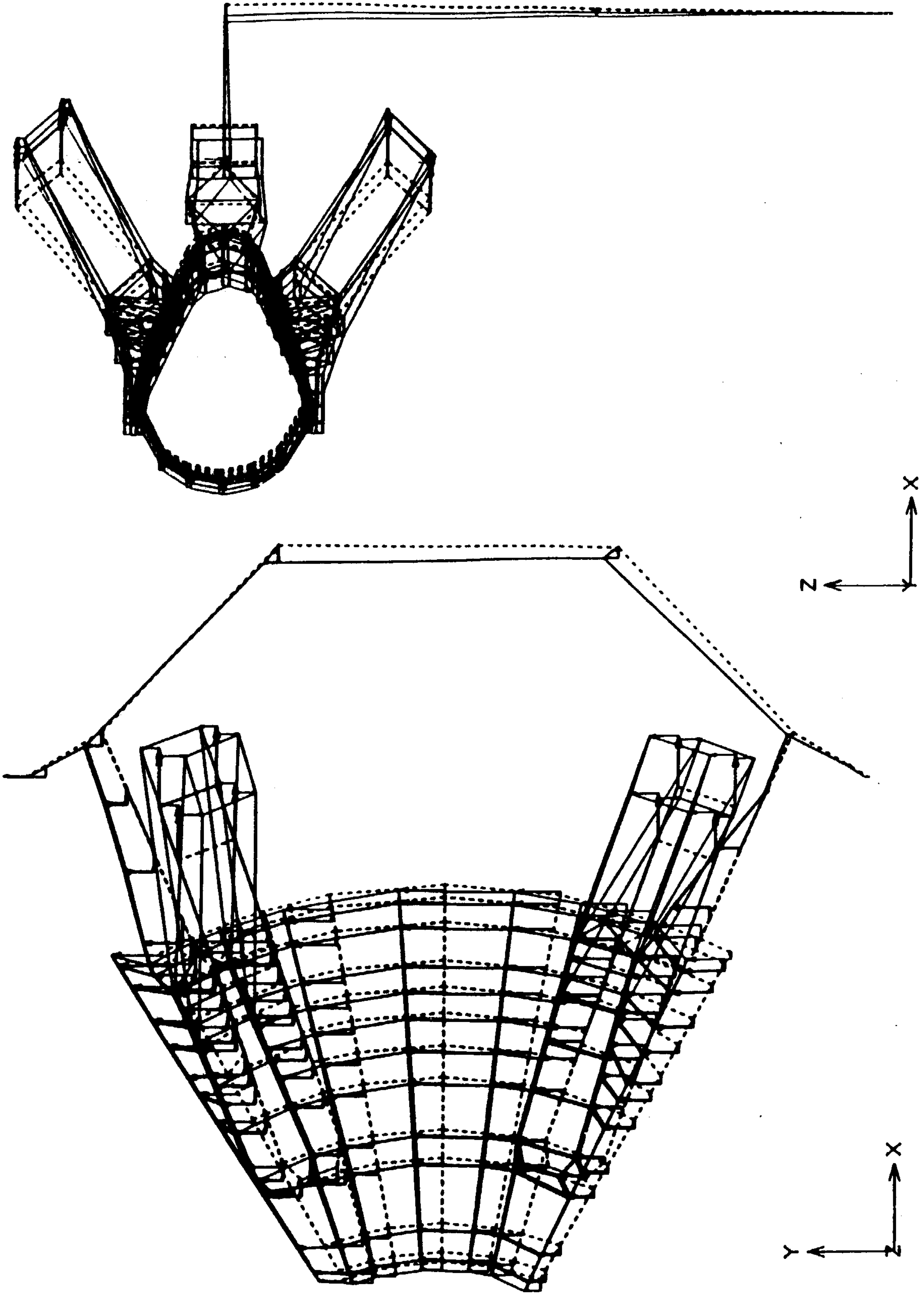

Fig. 6 1st eigenmode of the overall model.

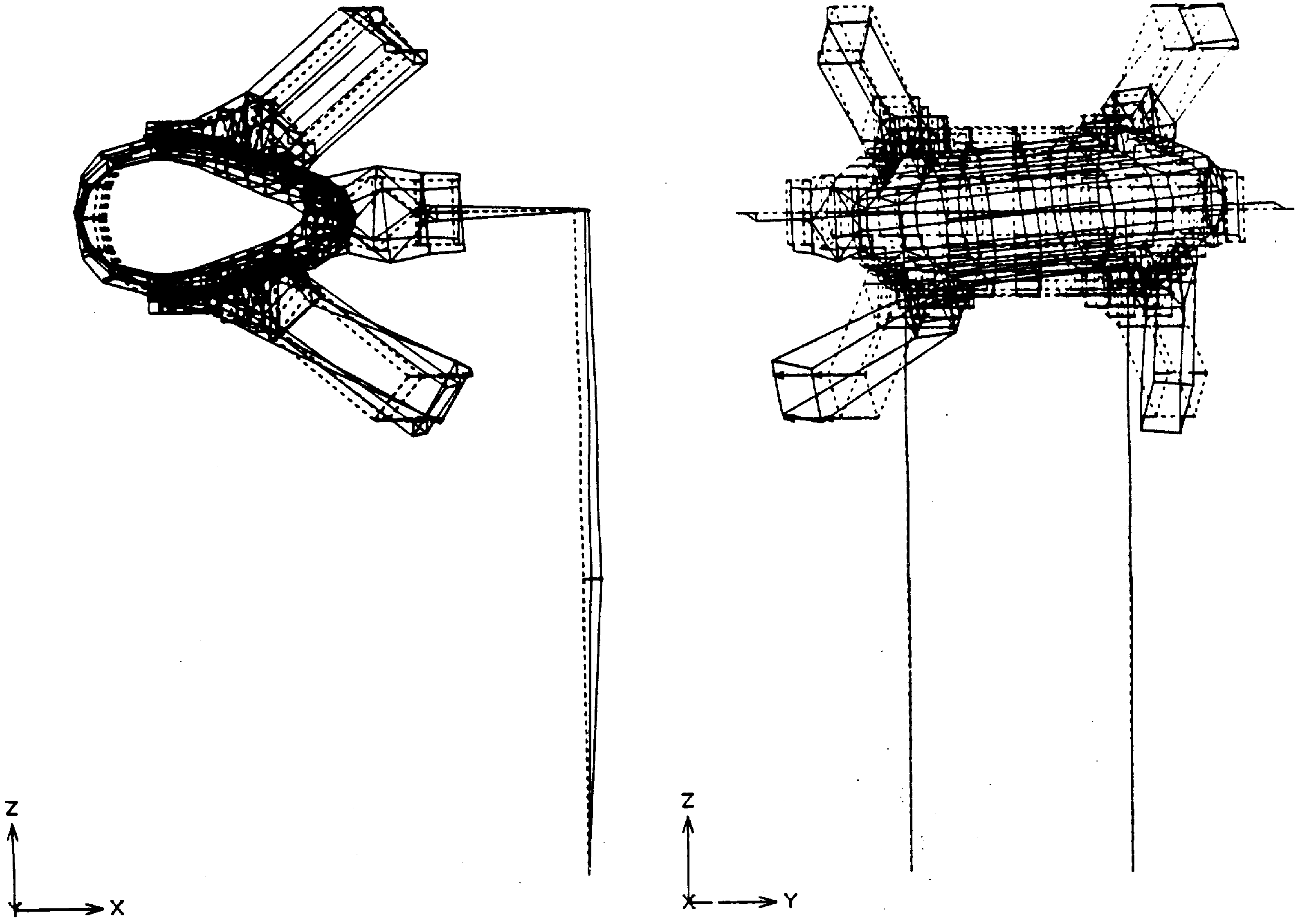

Fig. 7 8th eigenmode of the overall model.

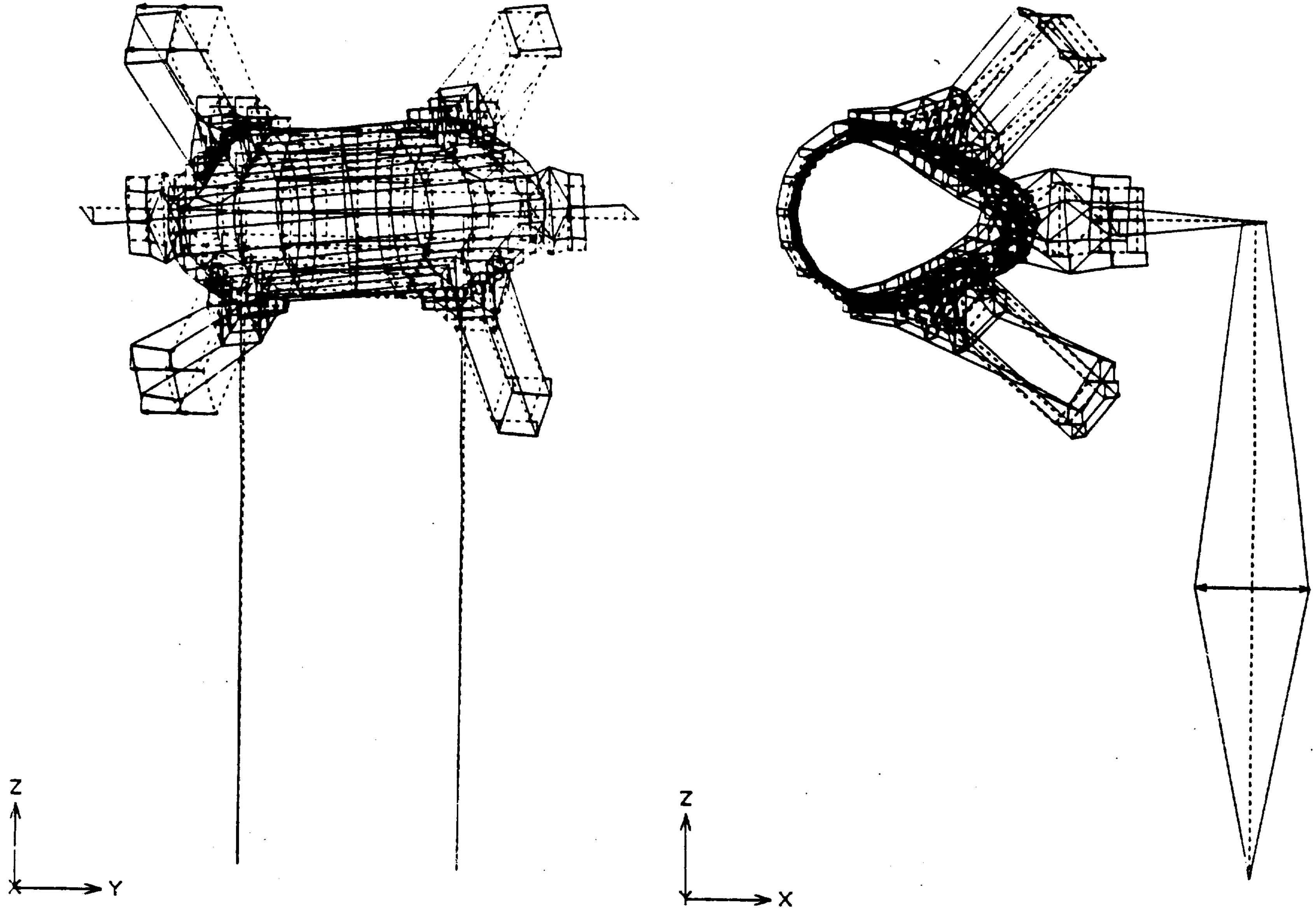

Fig. 8 14th eigenmode of the overall model.

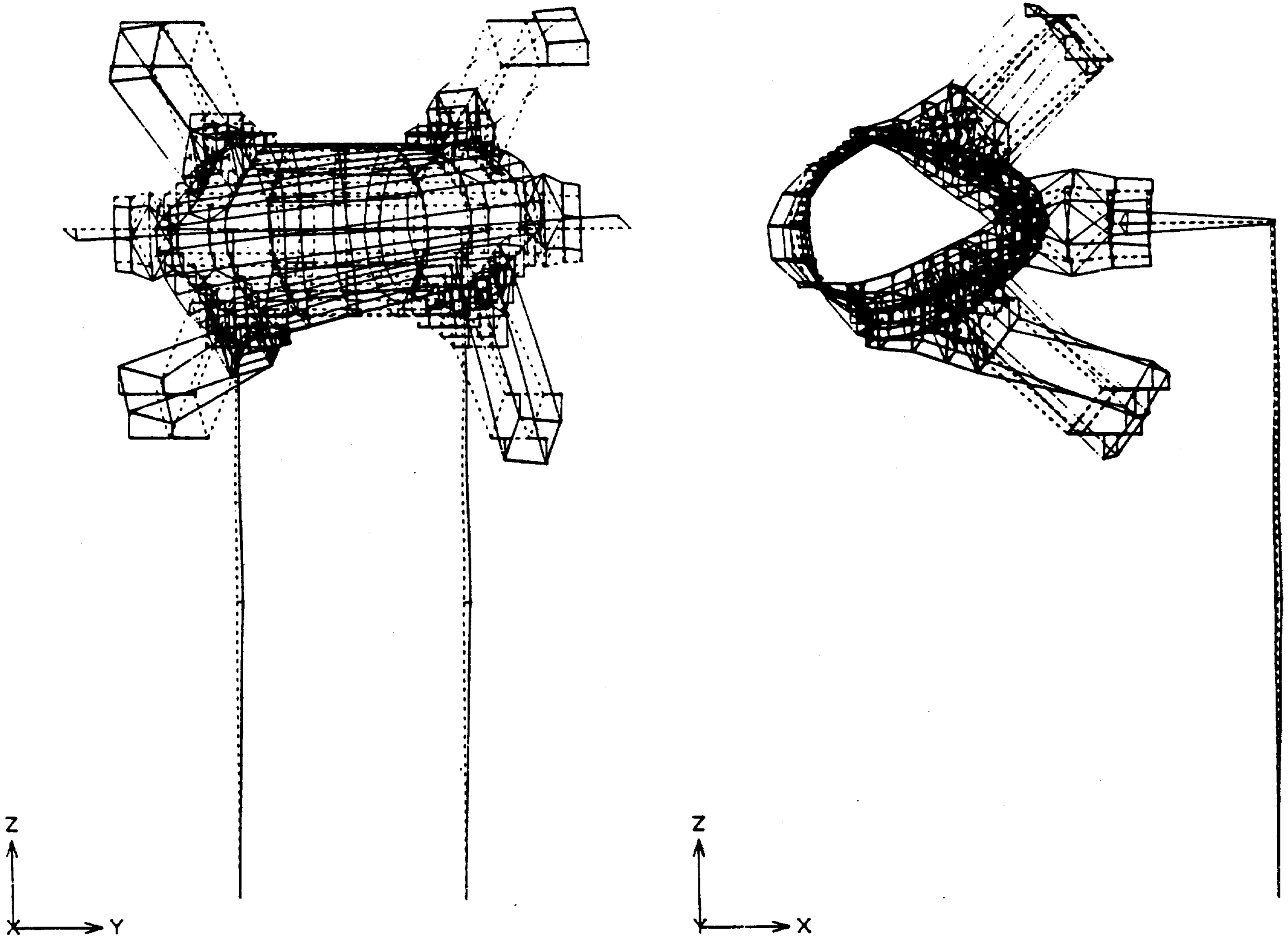

Fig. 9 20th eigenmode of the overall model.

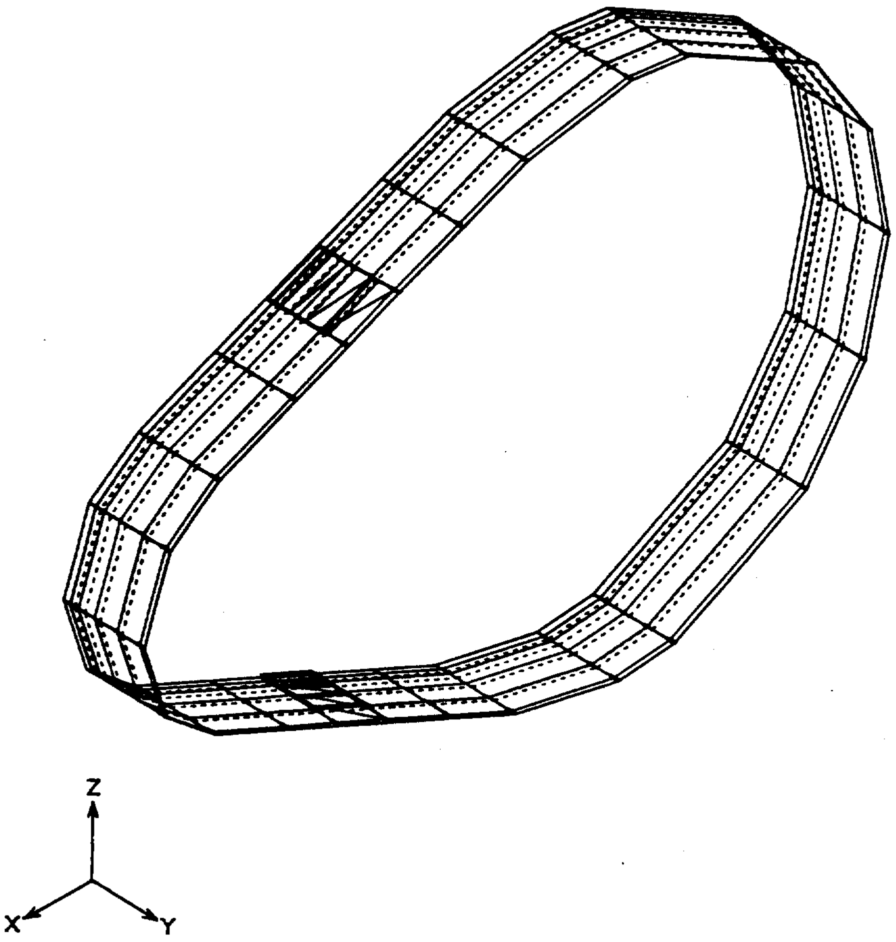

Fig.10 1st eigenmode of the bellows model.

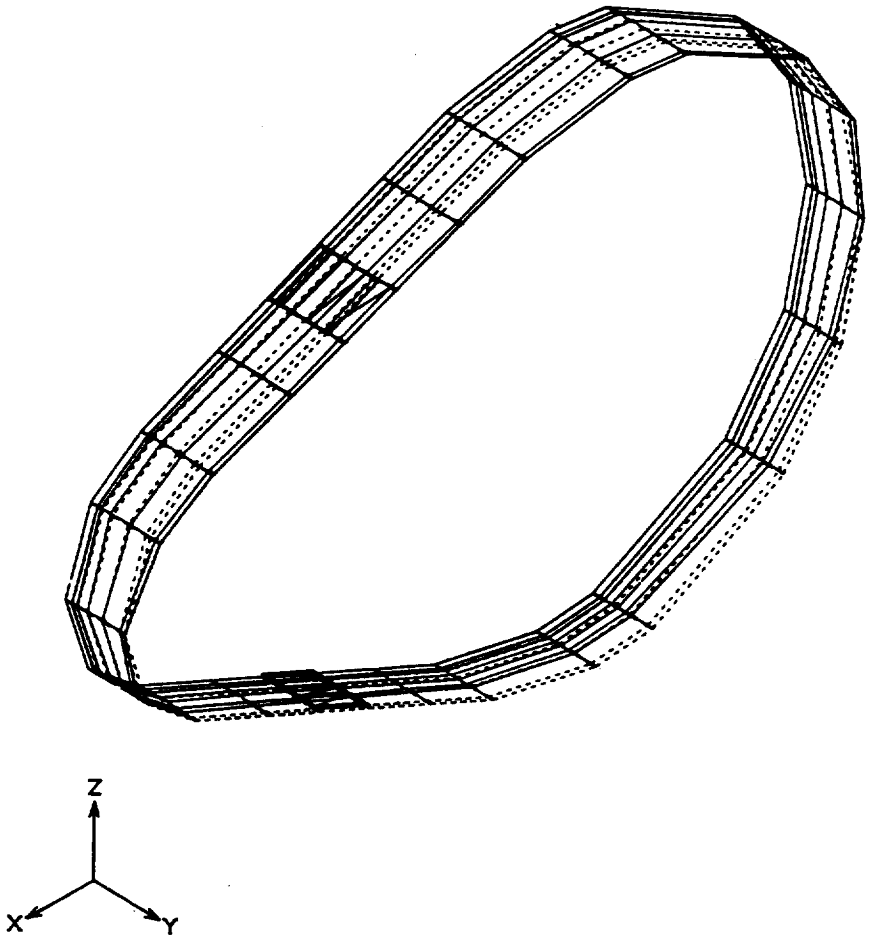

Fig.11 2nd eigenmode of the bellows model.

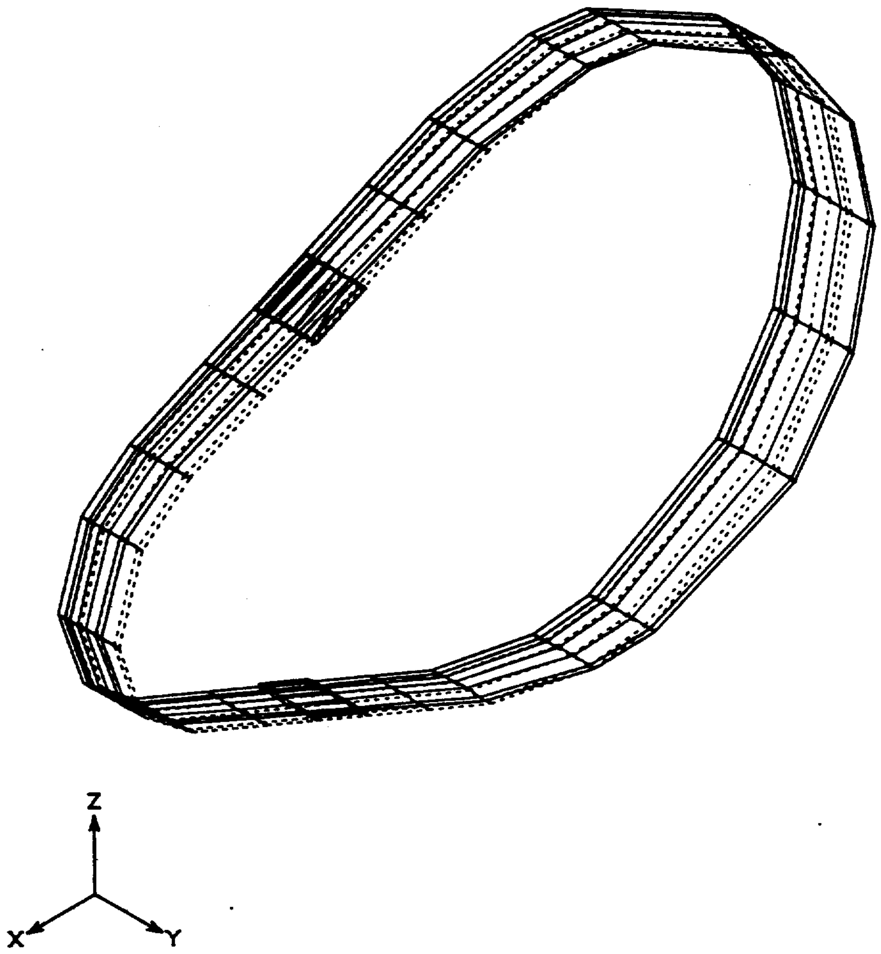

Fig.12 3rd eigenmode of the bellows model.

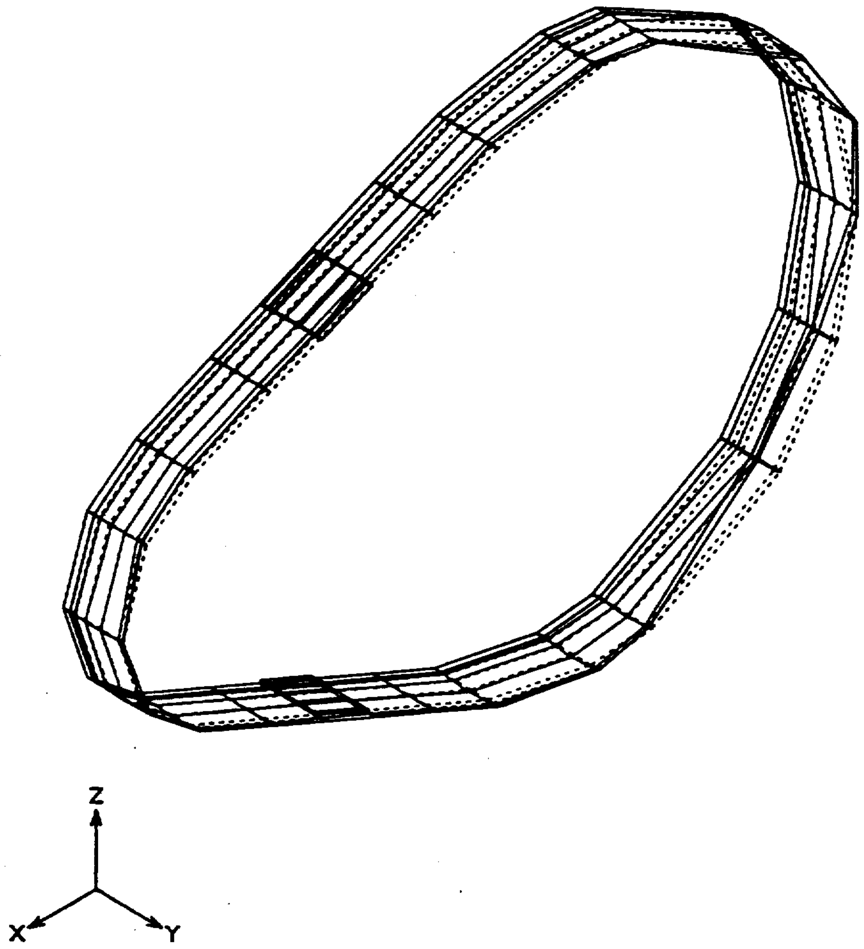

Fig.13 4th eigenmode of the bellows model.

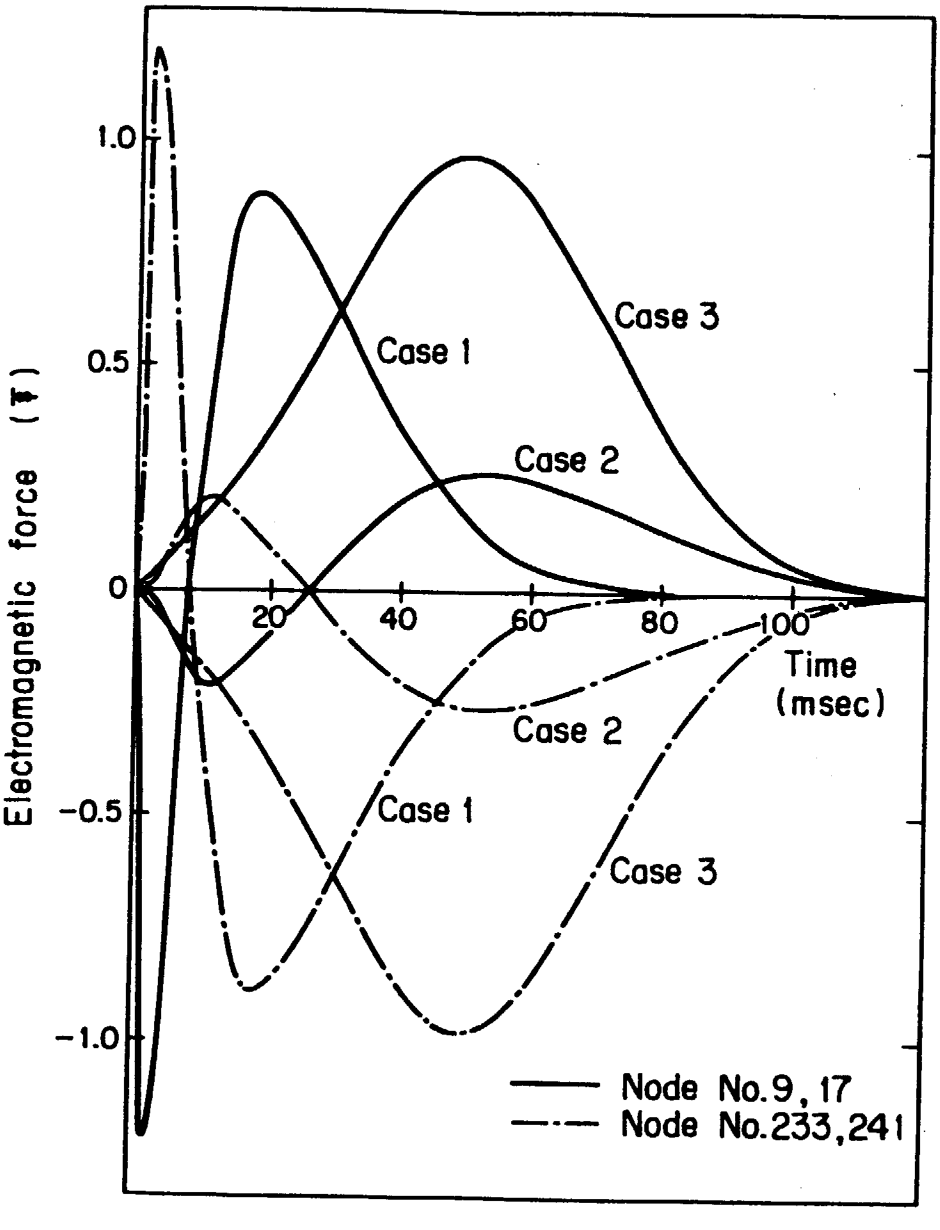

Fig.14 Time behaviors of the electromagnetic forces.

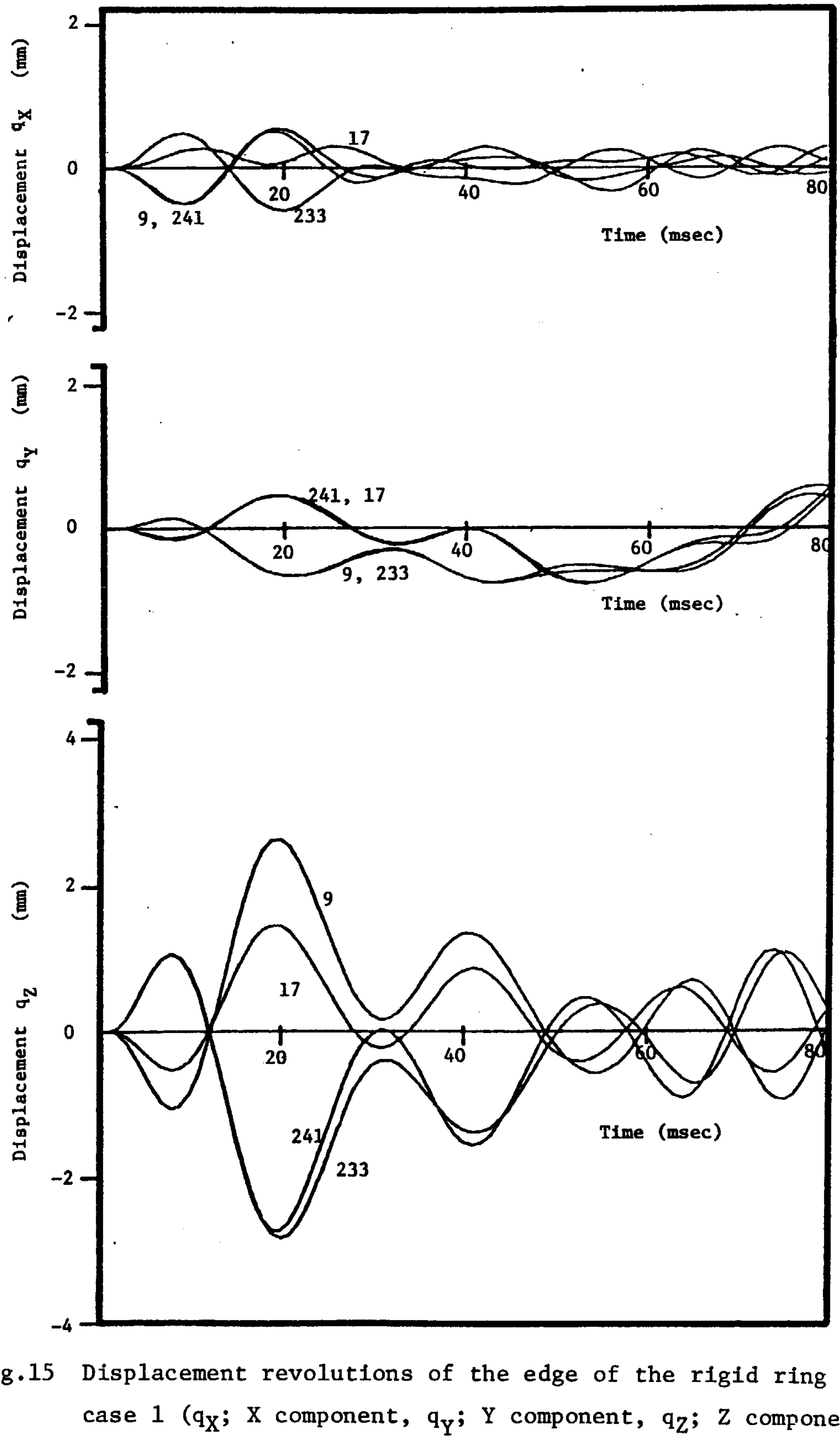

Fig.15 Displacement revolutions of the edge of the rigid ring for case 1 (q_X; X component, q_Y; Y component, q_Z; Z component).

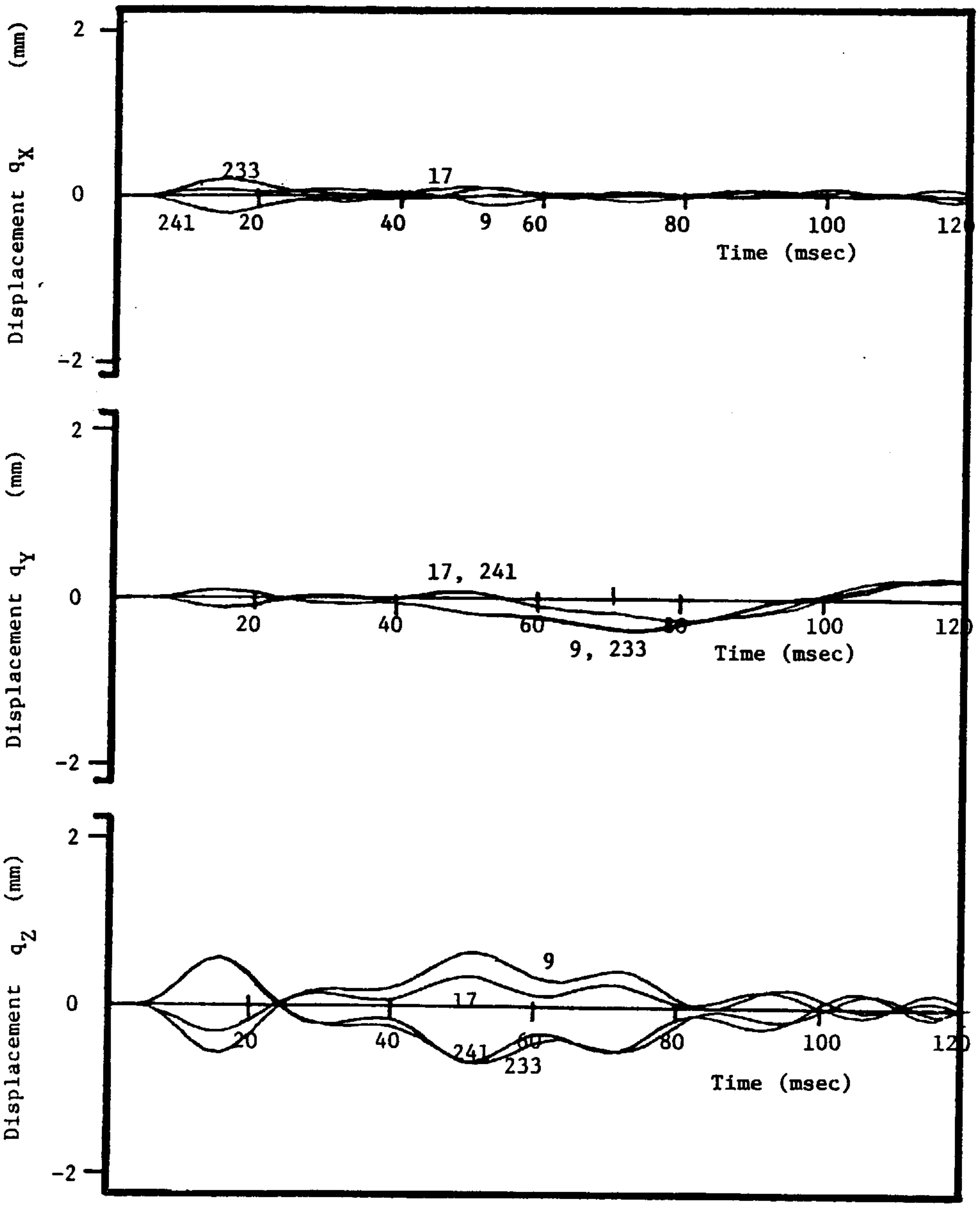

Fig.16 Displacement revolutions of the edge of the rigid ring for case 2.

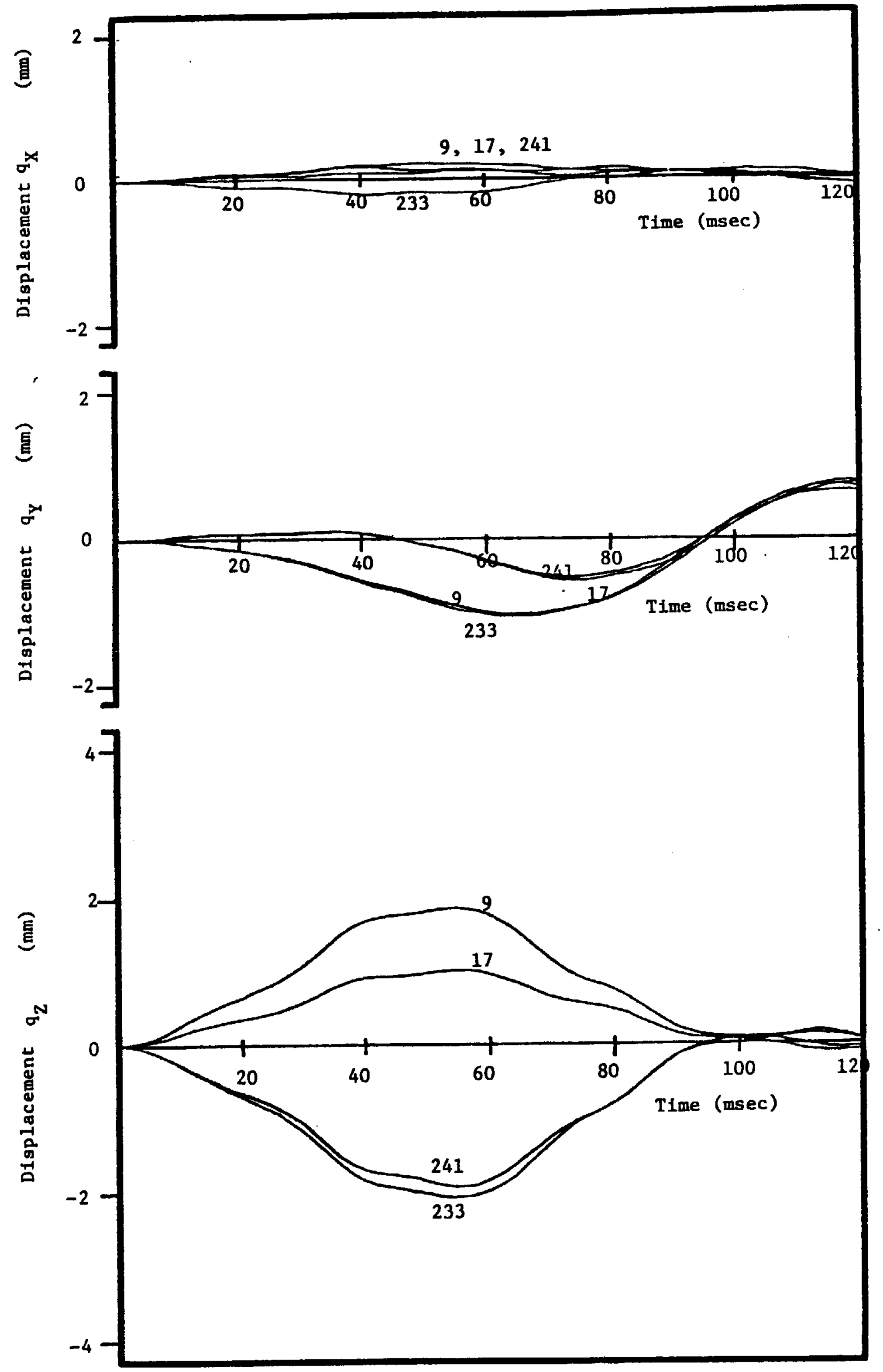

Fig.17 Displacement revolutions of the edge of the rigid ring for case 3.

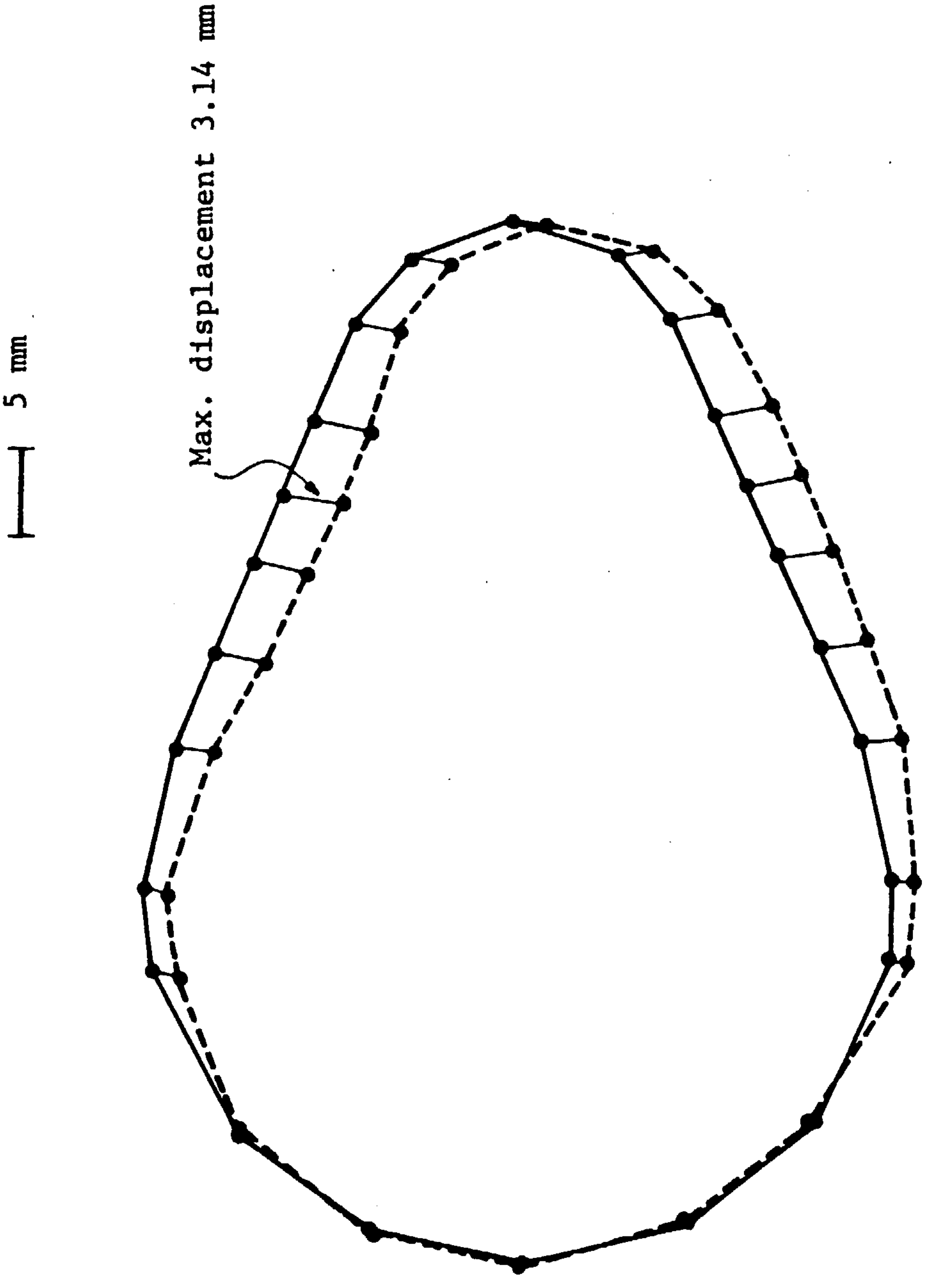

Fig.18 Poloidal distribution of the displacement at the edge of the rigid ring for case 1 at the time of maximum displacement occurrence.

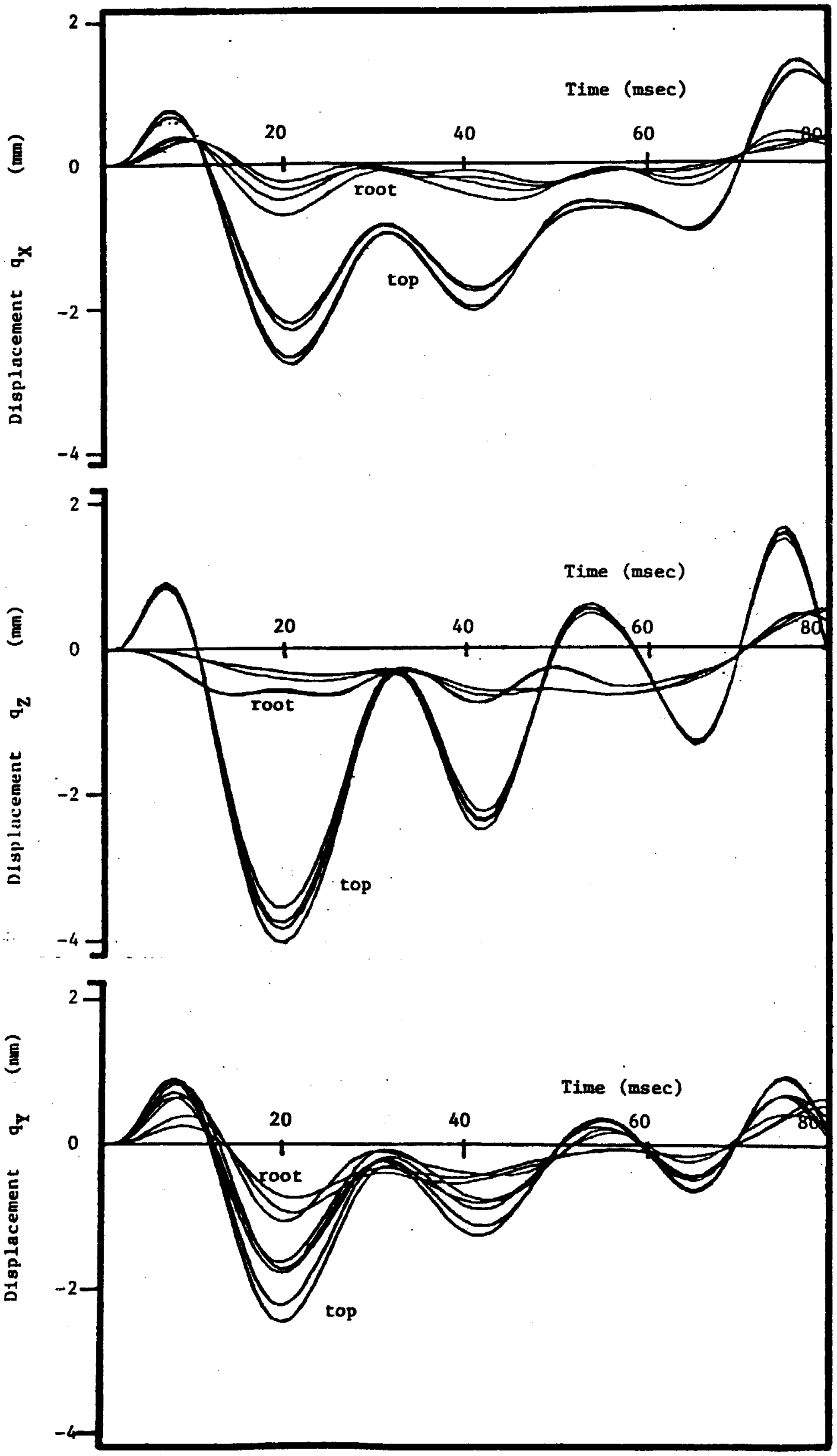

Fig.19 Displacement revolutions of the top and the root of the ports for case 1.

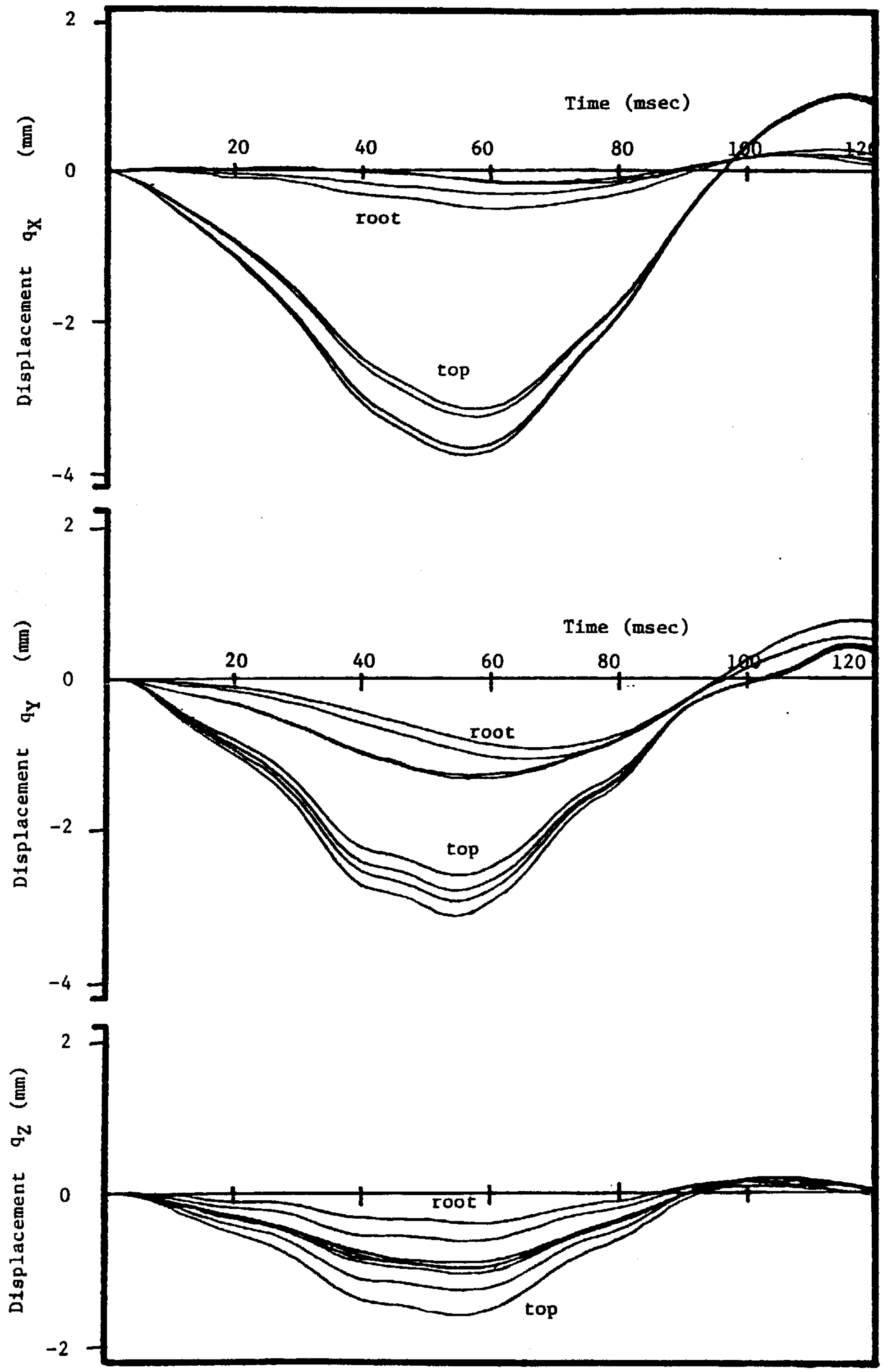

Fig.20 Displacement revolutions of the top and the root of the ports for case 3.

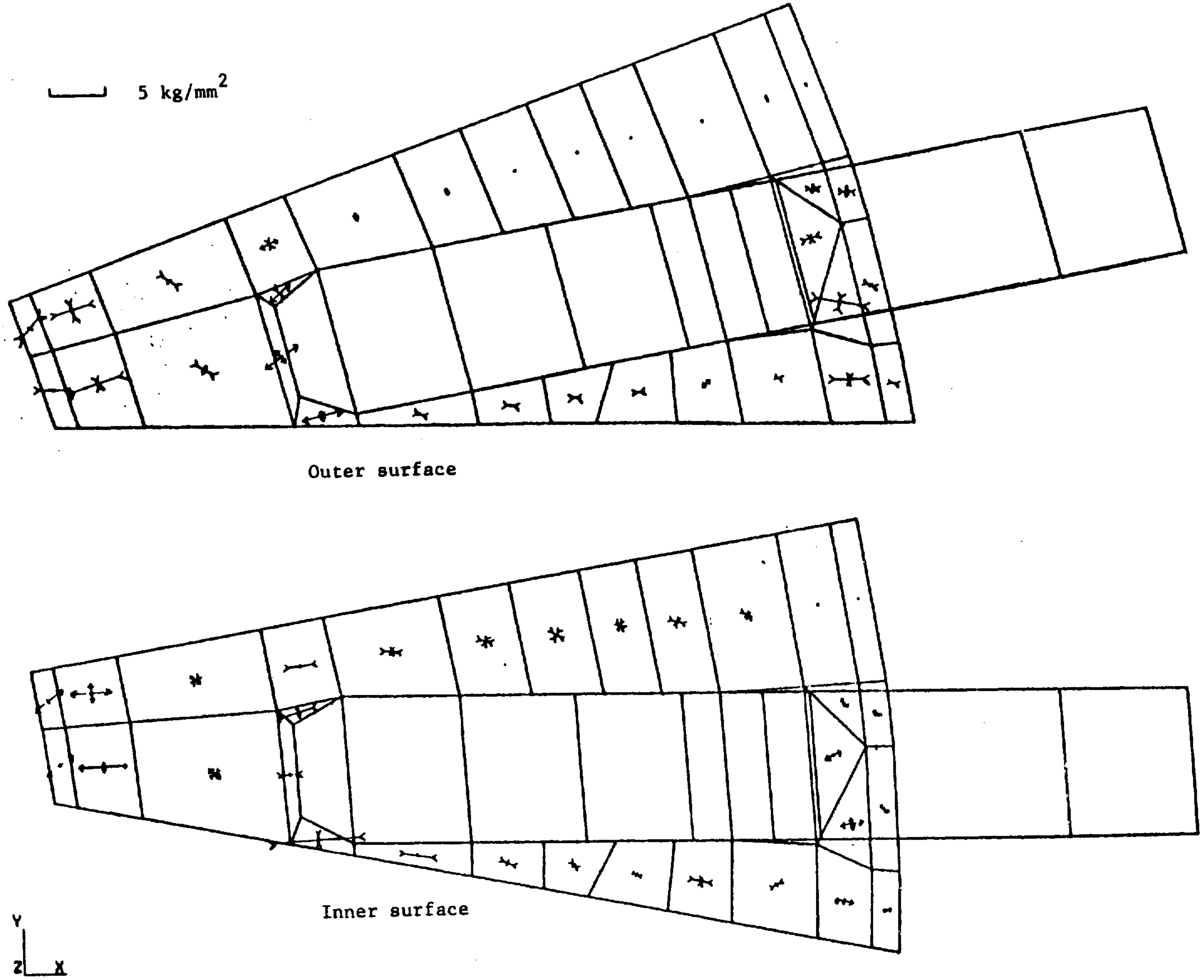

Outer surface

Inner surface

Fig.21 Stress distribution of the outer and the inner surfaces of the rigid ring for case 1 (t = 12 msec).

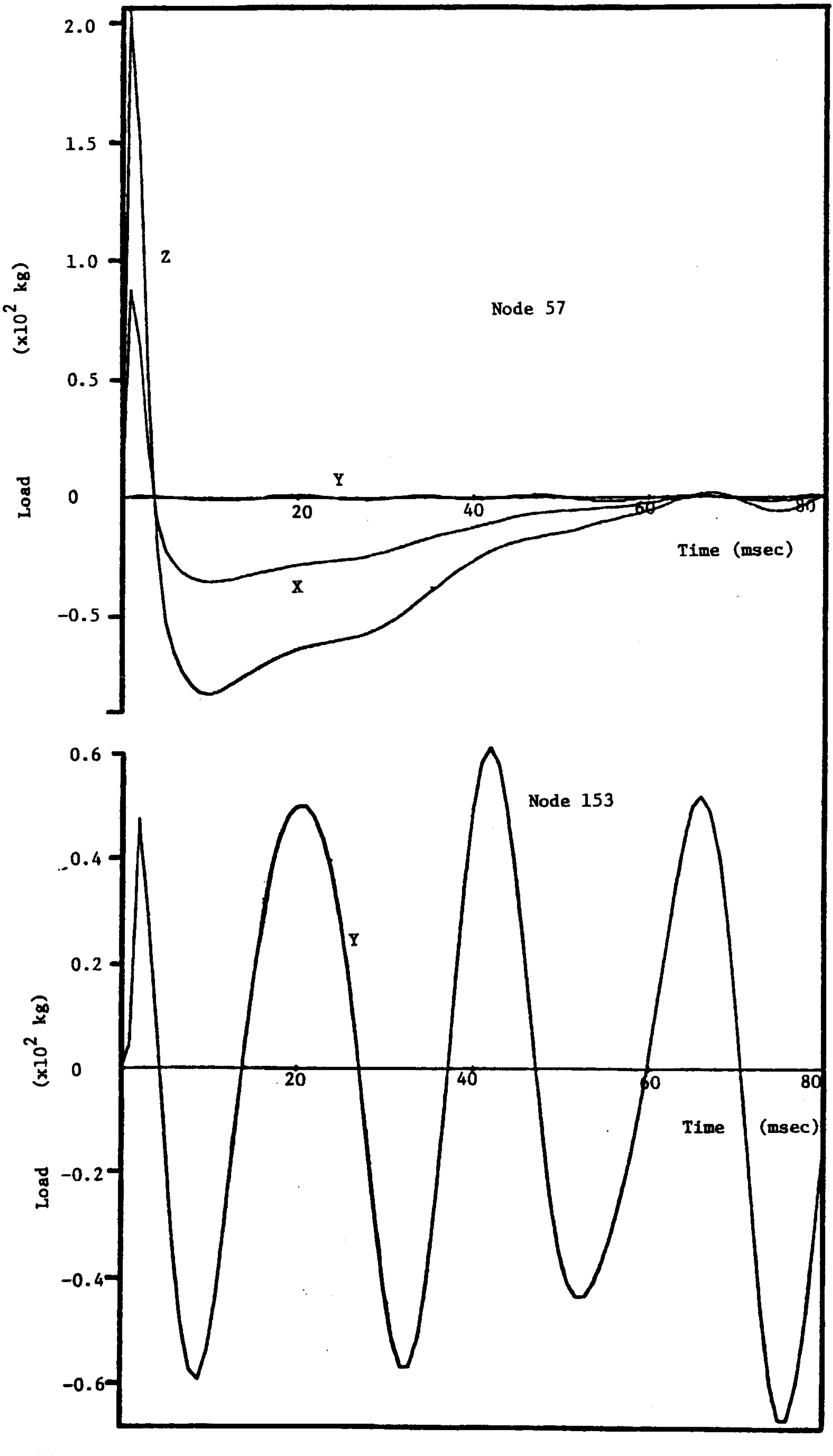

Fig.22 Time behaviors of the load acting on the nodal points 57 and 153 for case 1.

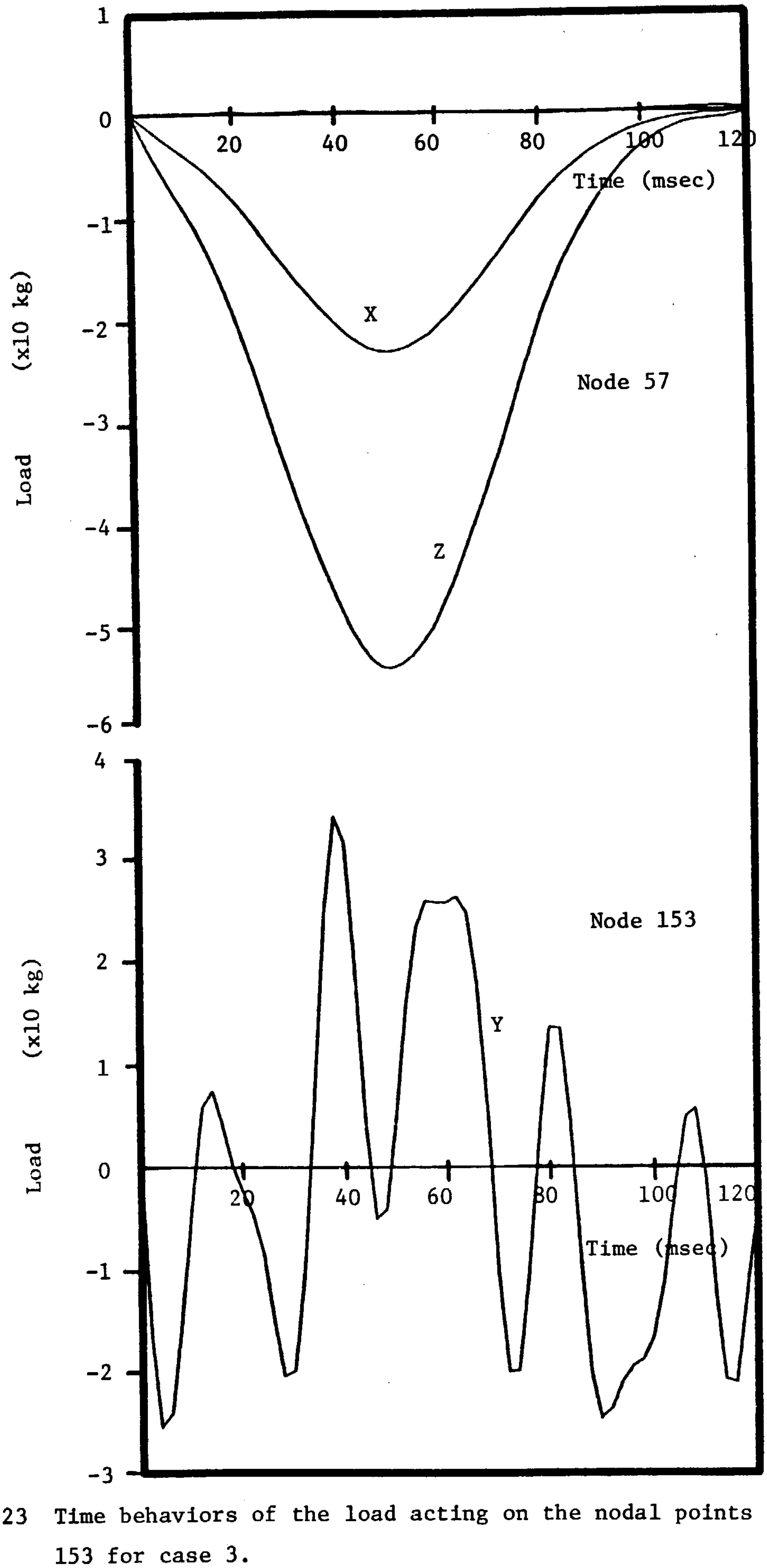

Fig.23 Time behaviors of the load acting on the nodal points 57 and 153 for case 3.

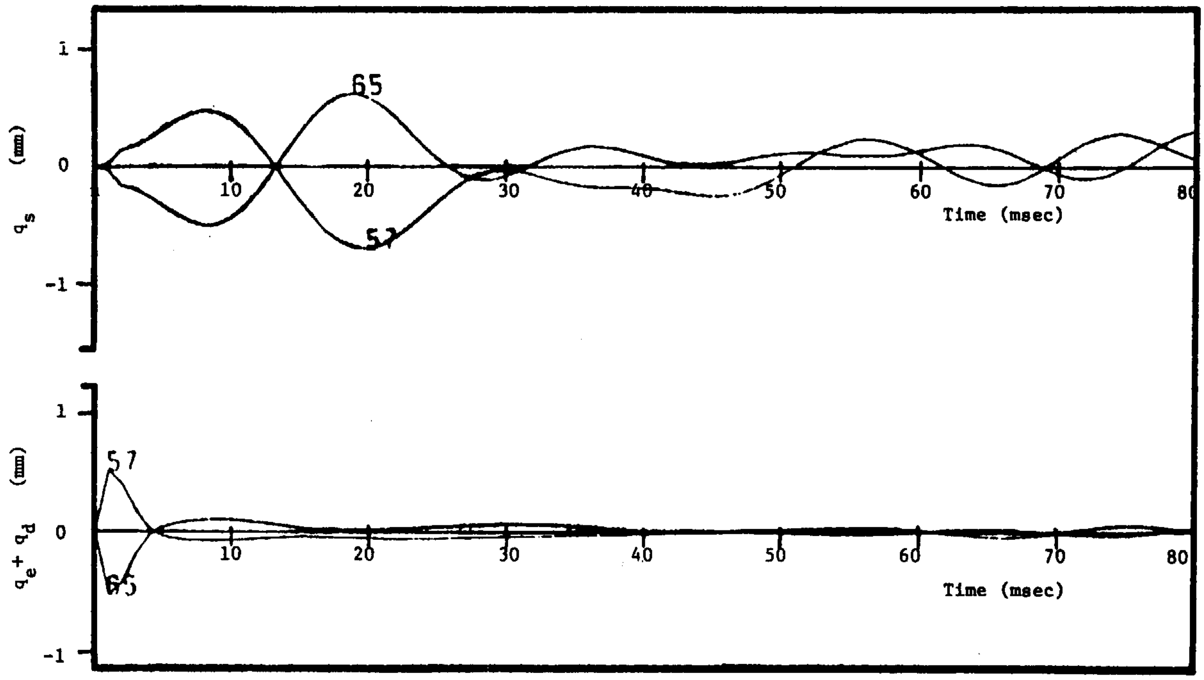

Fig.24 Time behaviors of X components of q_s and $q_e + q_d$ of the bellows for case 1.

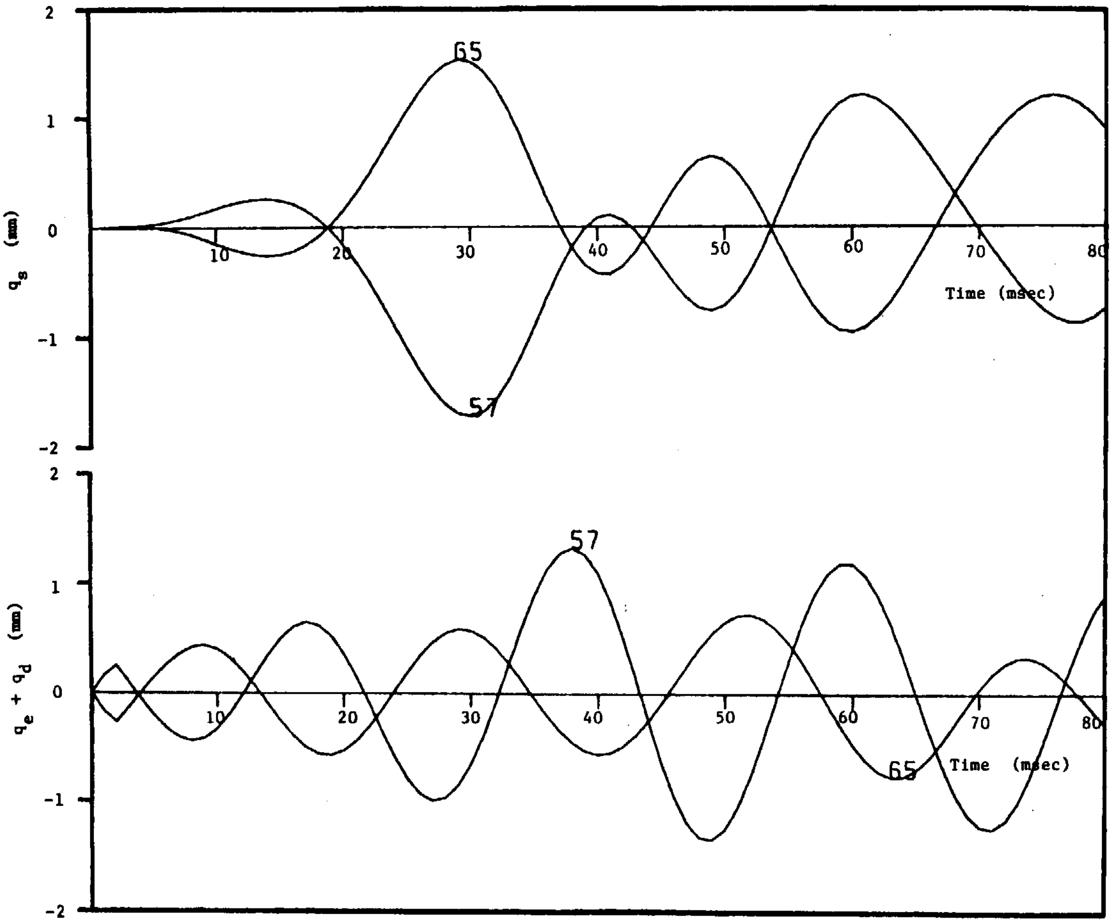

Fig.25 Time behaviors of Y components of q_s and $q_e + q_d$ of the bellows for case 1.

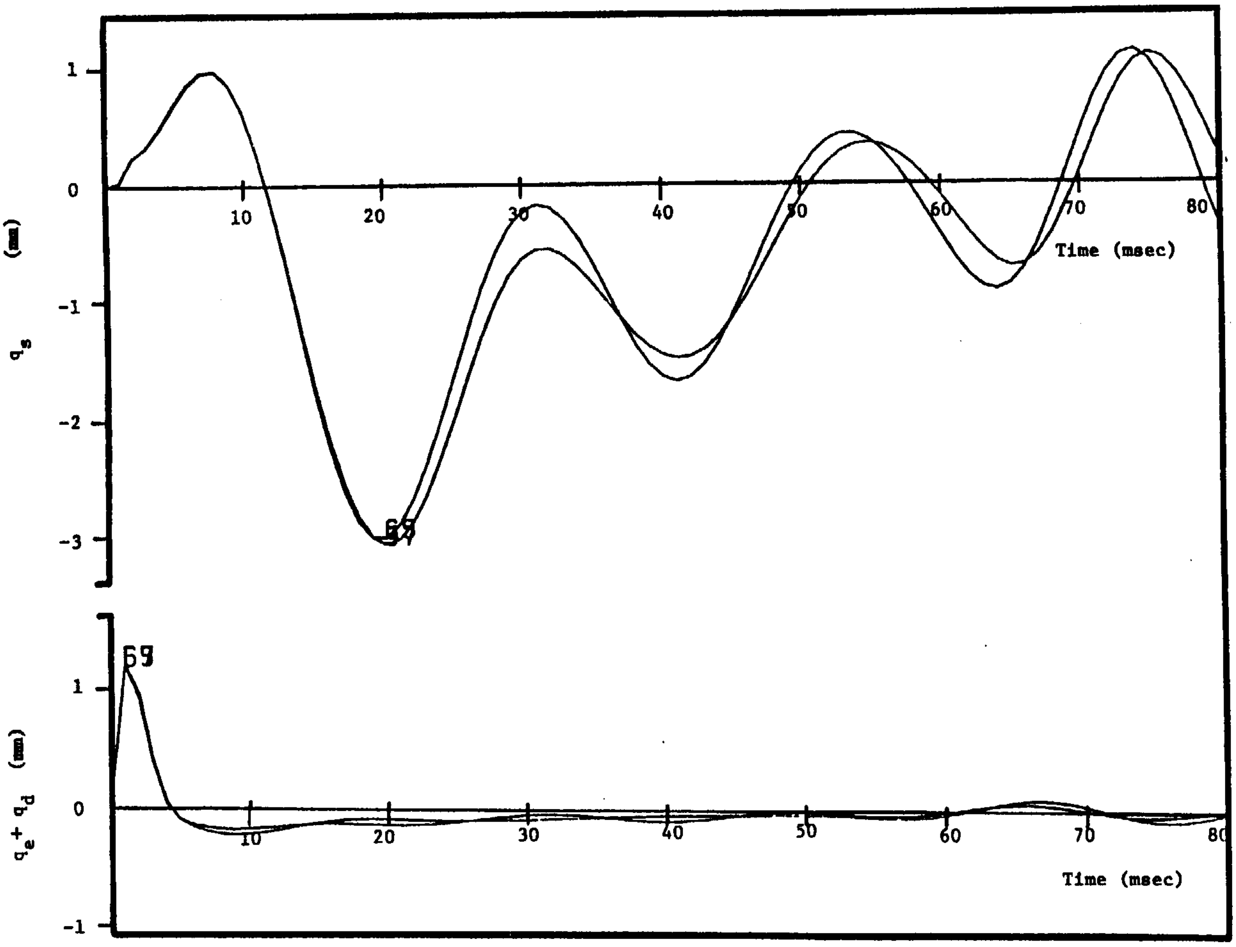

Fig.26 Time behaviors of Z components of q_s and q_e+q_d of the bellows for case 1.

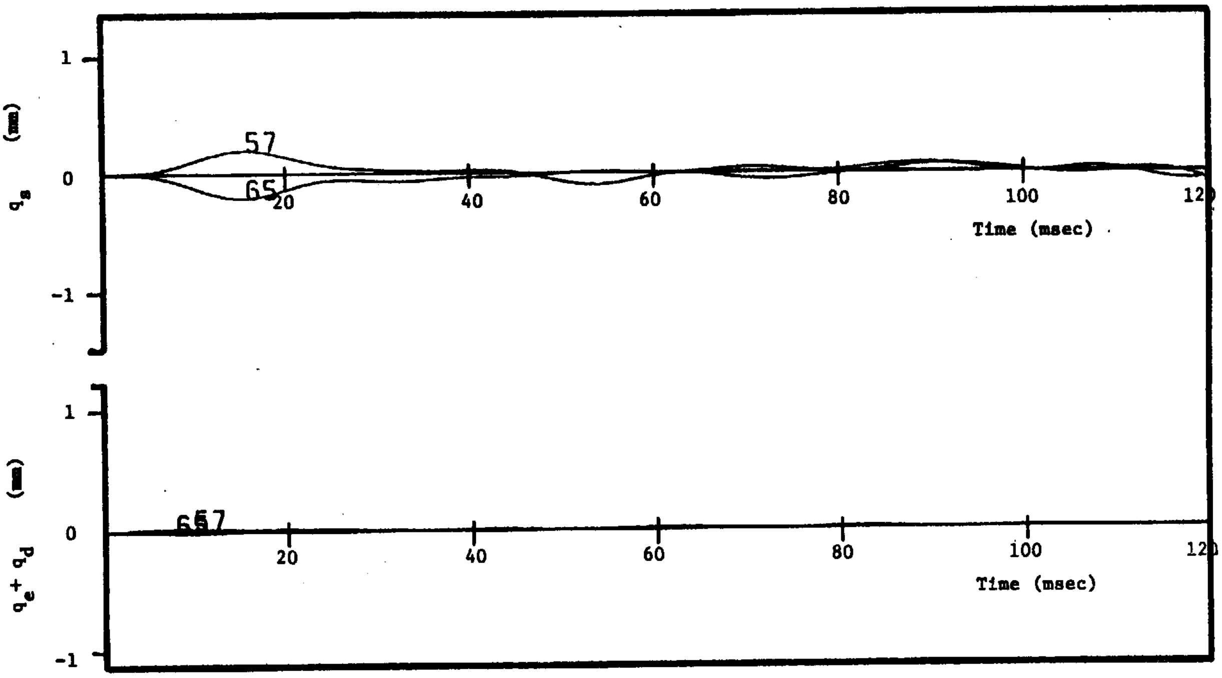

Fig.27 Time behaviors of X components of q_s and q_e+q_d of the bellows for case 2.

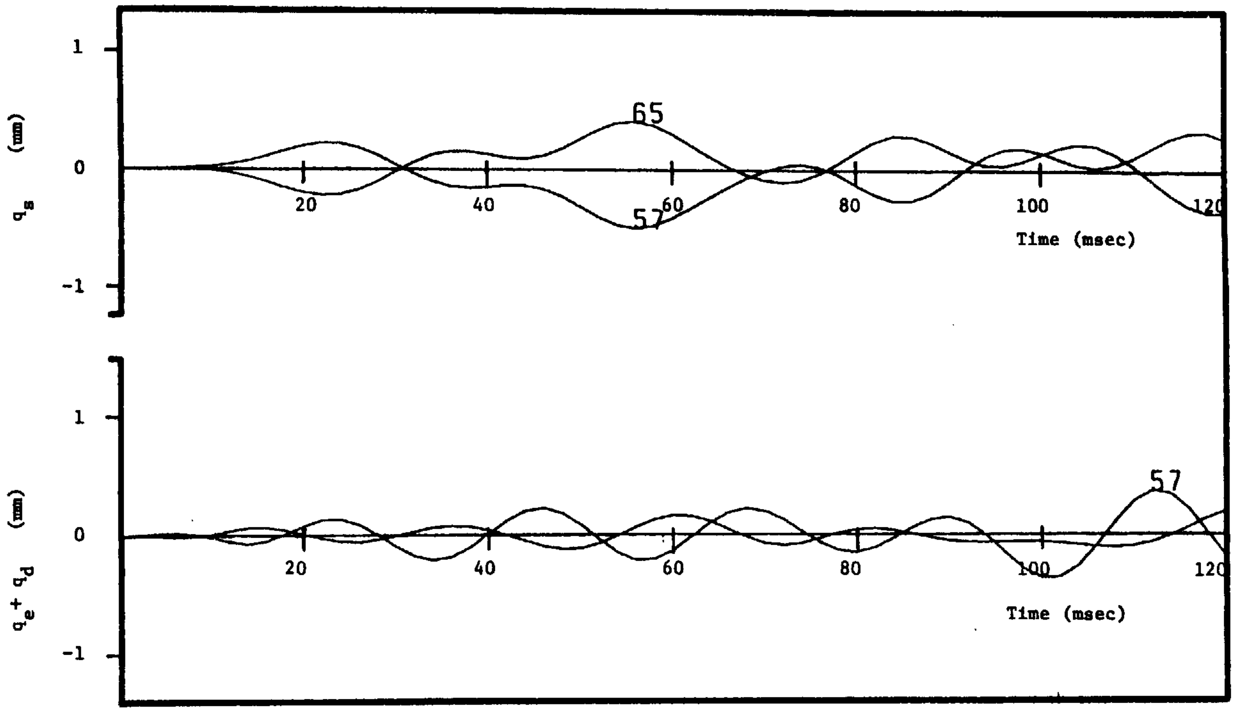

Fig.28 Time behaviors of Y components of q_s and $q_e + q_d$ of the bellows for case 2.

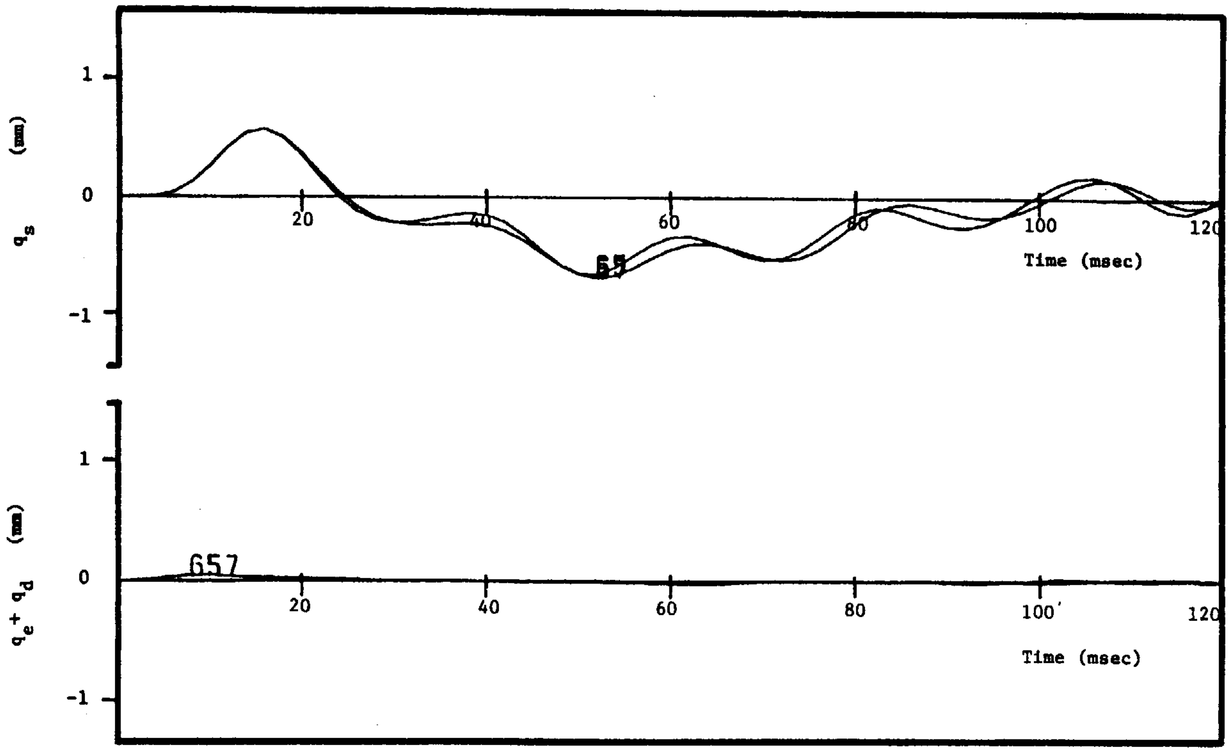

Fig.29 Time behaviors of Z components of q_s and $q_e + q_d$ of the bellows for case 2.

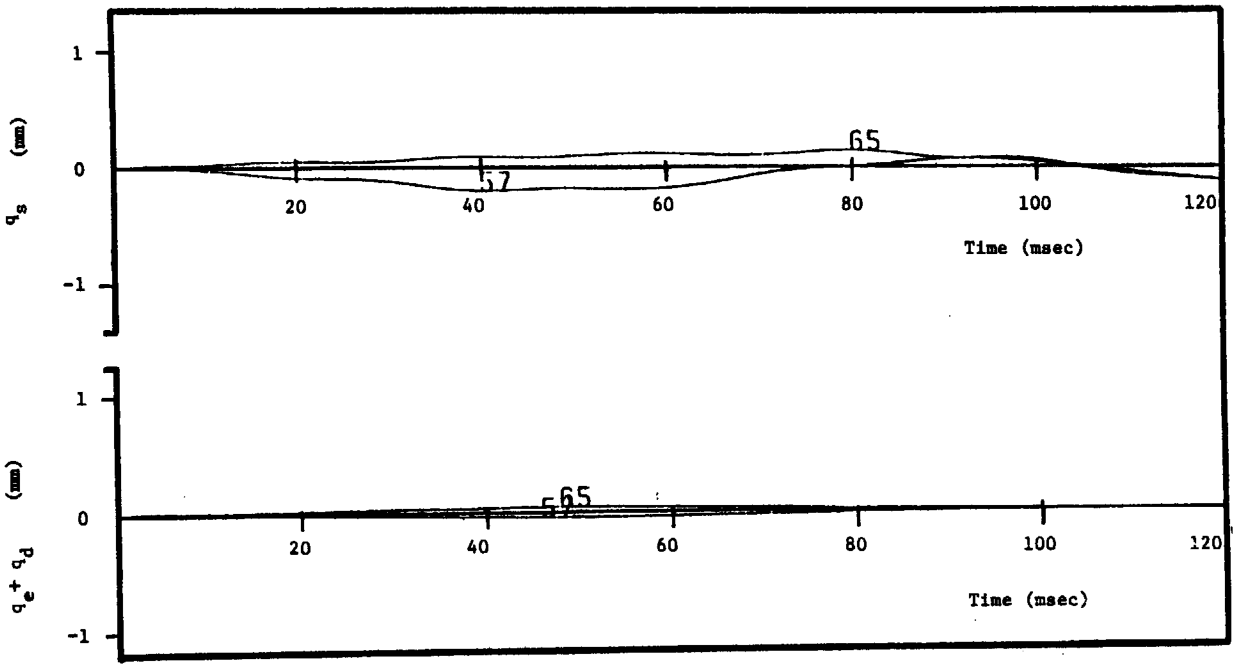

Fig.30 Time behaviors of X components of q_s and $q_e + q_d$ of the bellows for case 3.

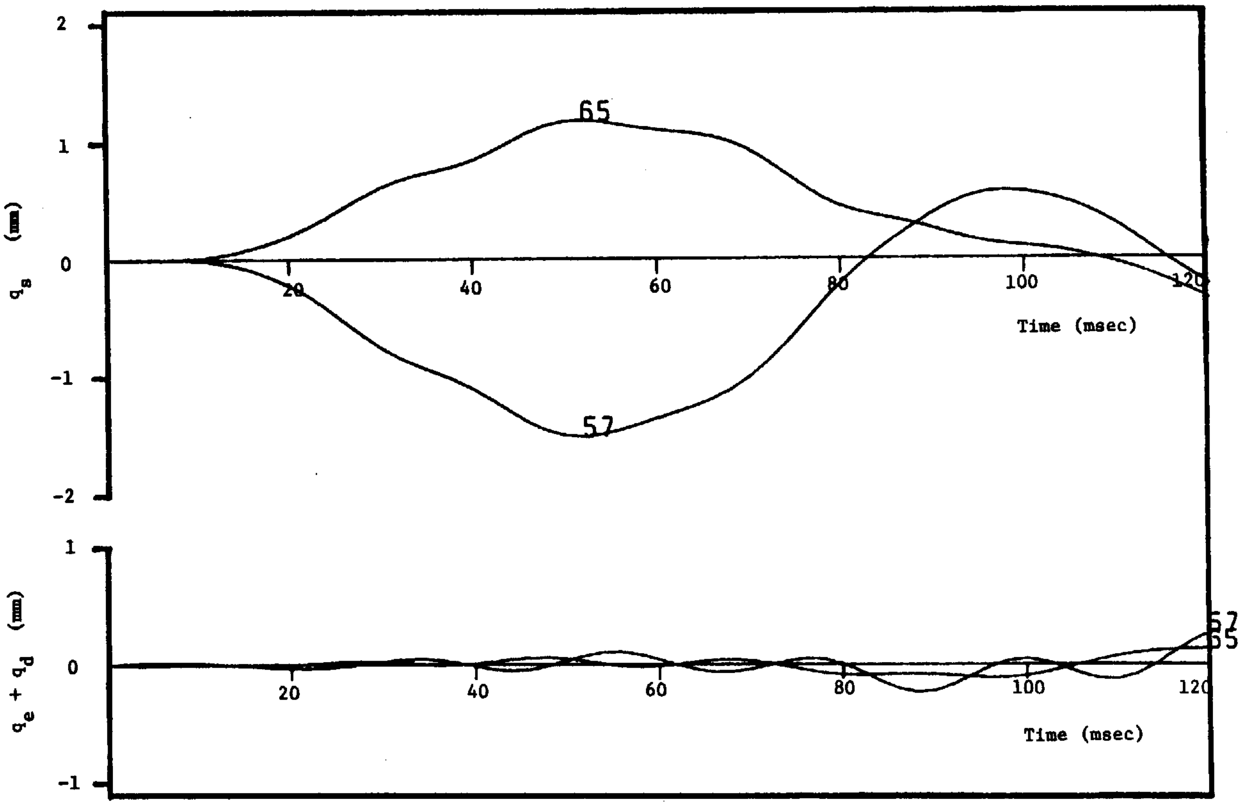

Fig.31 Time behaviors of Y components of q_s and $q_e + q_d$ of the bellows for case 3.

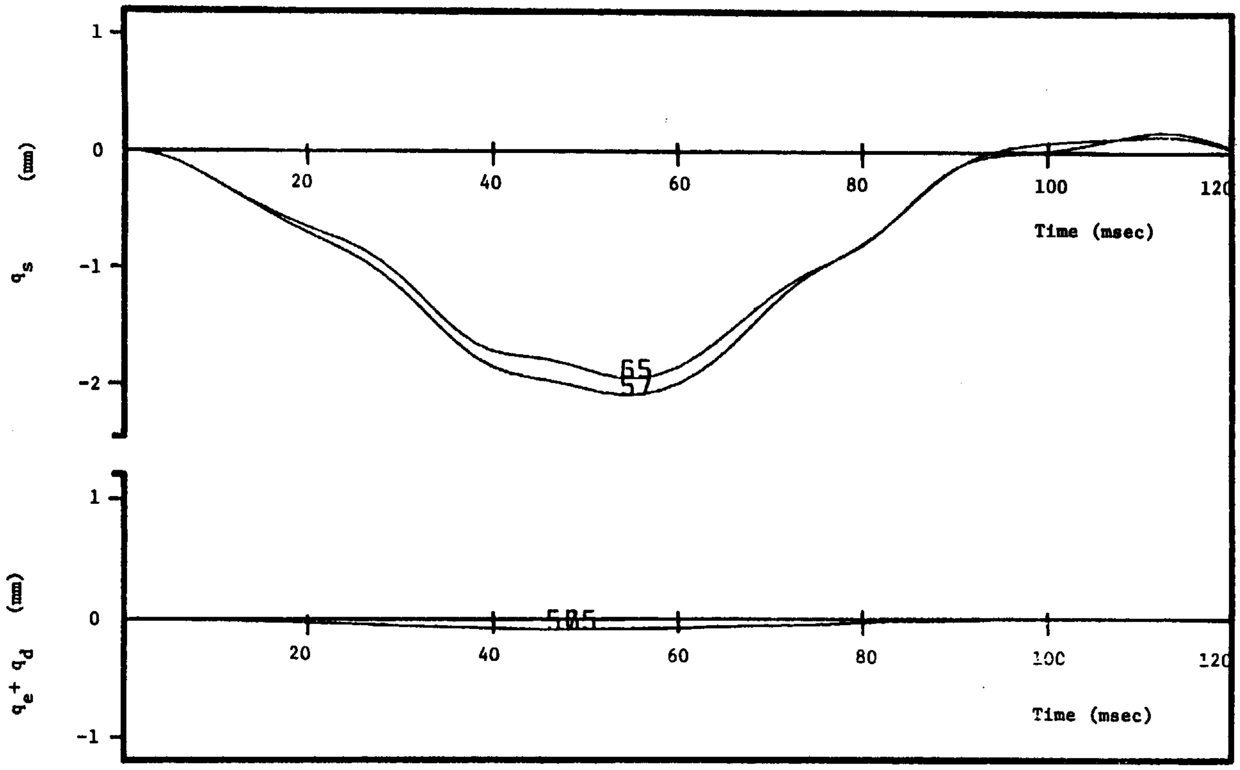

Fig.32 Time behaviors of Z components of q_s and $q_e + q_d$ of the bellows for case 3.

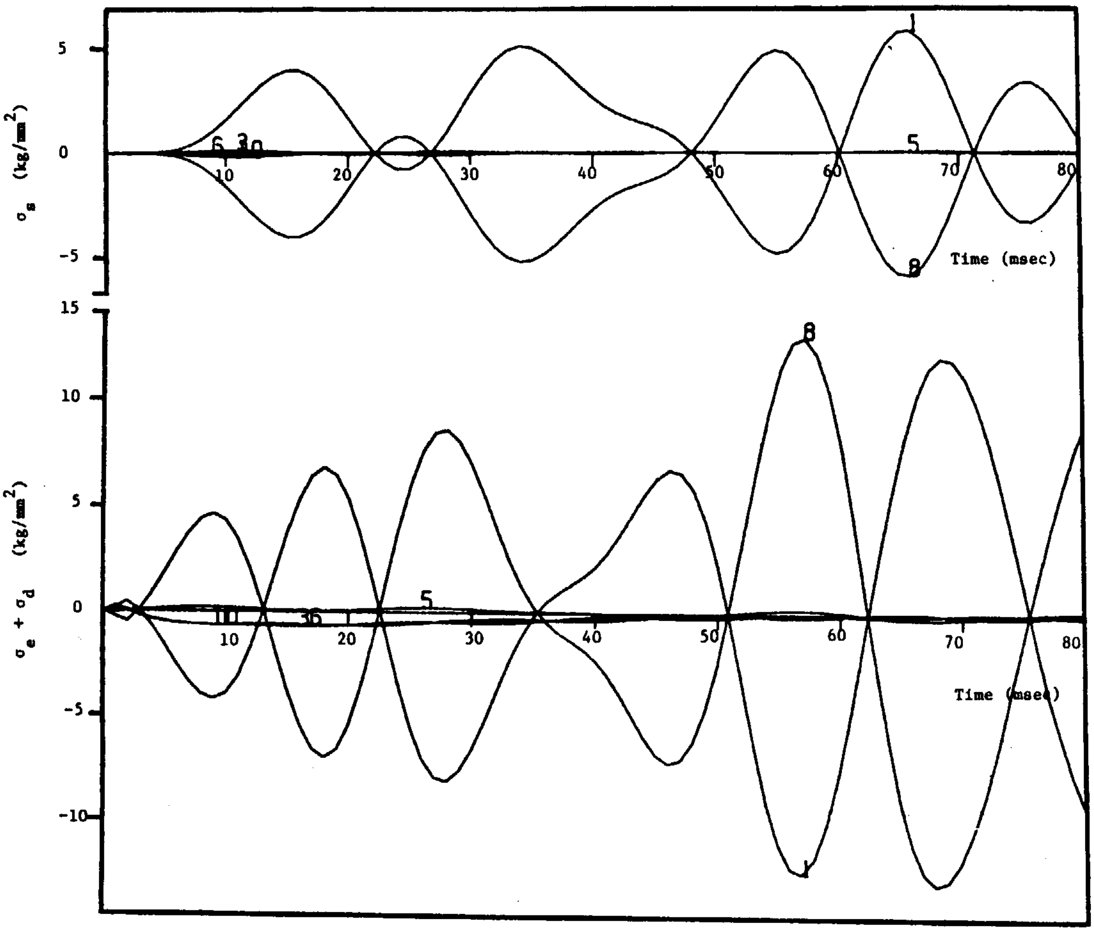

Fig.33 Time behaviors of σ_s and $\sigma_e + \sigma_d$ of the bellows for case 1 (element 26).

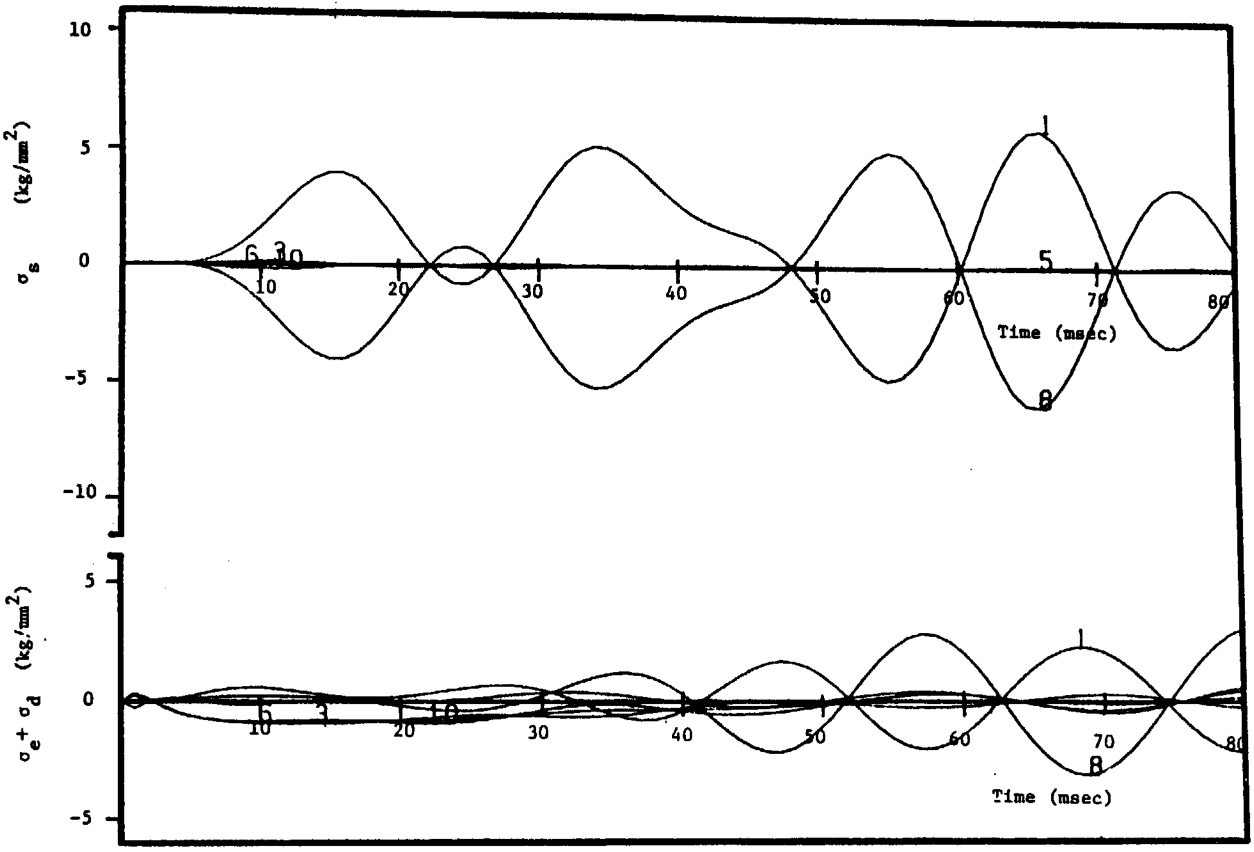

Fig.34 Time behaviors of σ_s and $\sigma_e + \sigma_d$ of the bellows for case 1 (element 122).

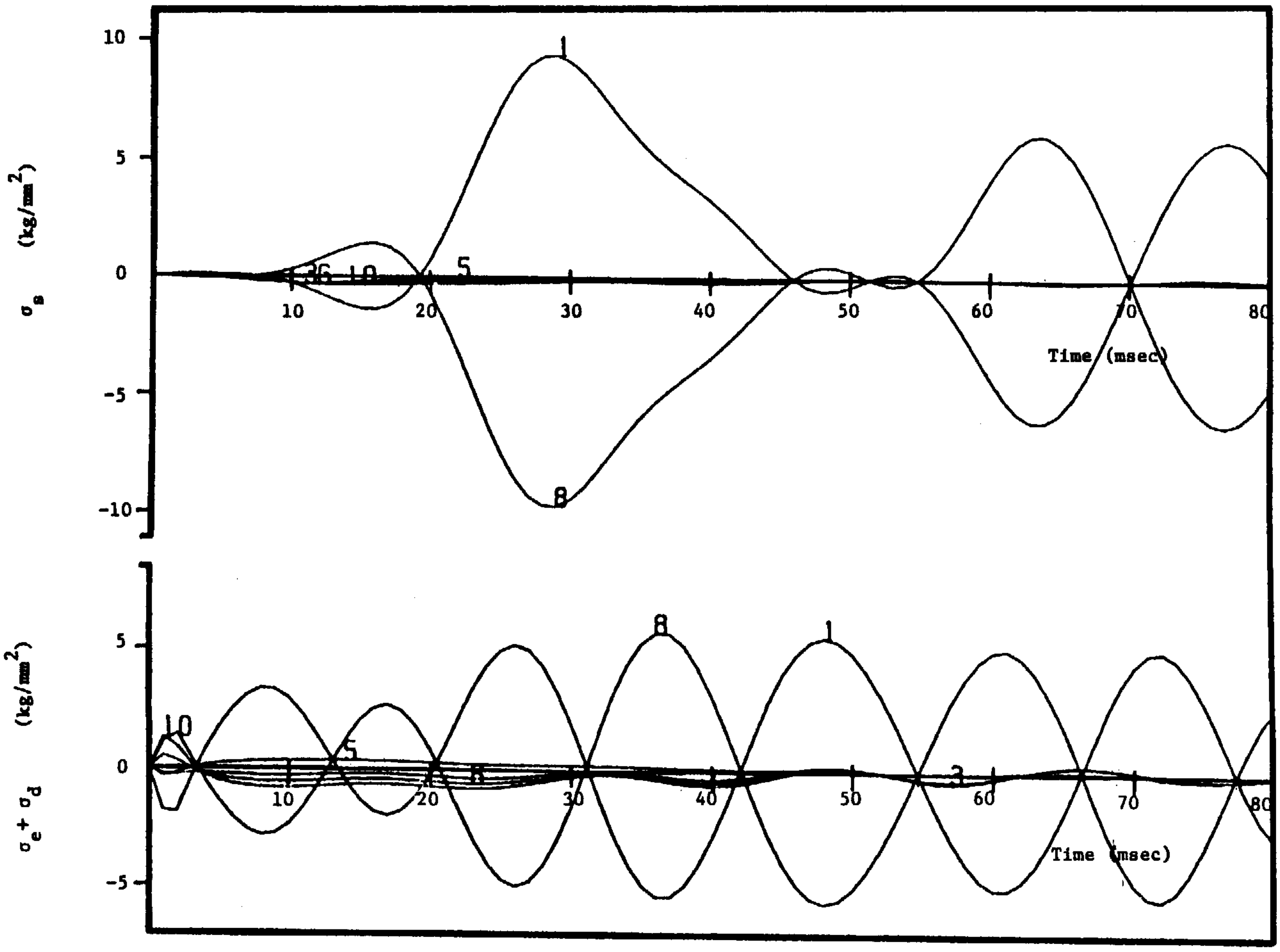

Fig.35 Time behaviors of σ_s and $\sigma_e + \sigma_d$ of the bellows for case 1 (element 31).

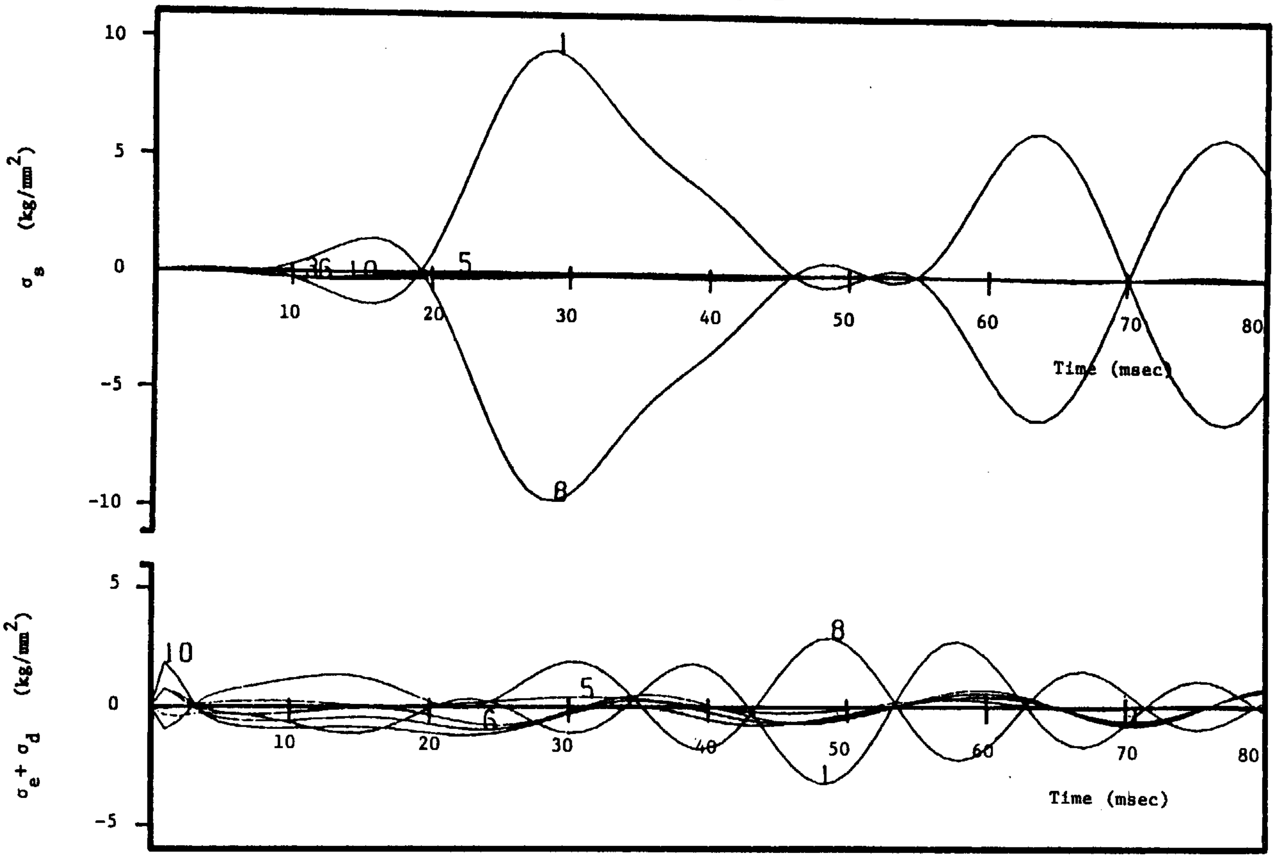

Fig.36 Time behaviors of σ_s and $\sigma_e + \sigma_d$ of the bellows for case 1 (element 127).

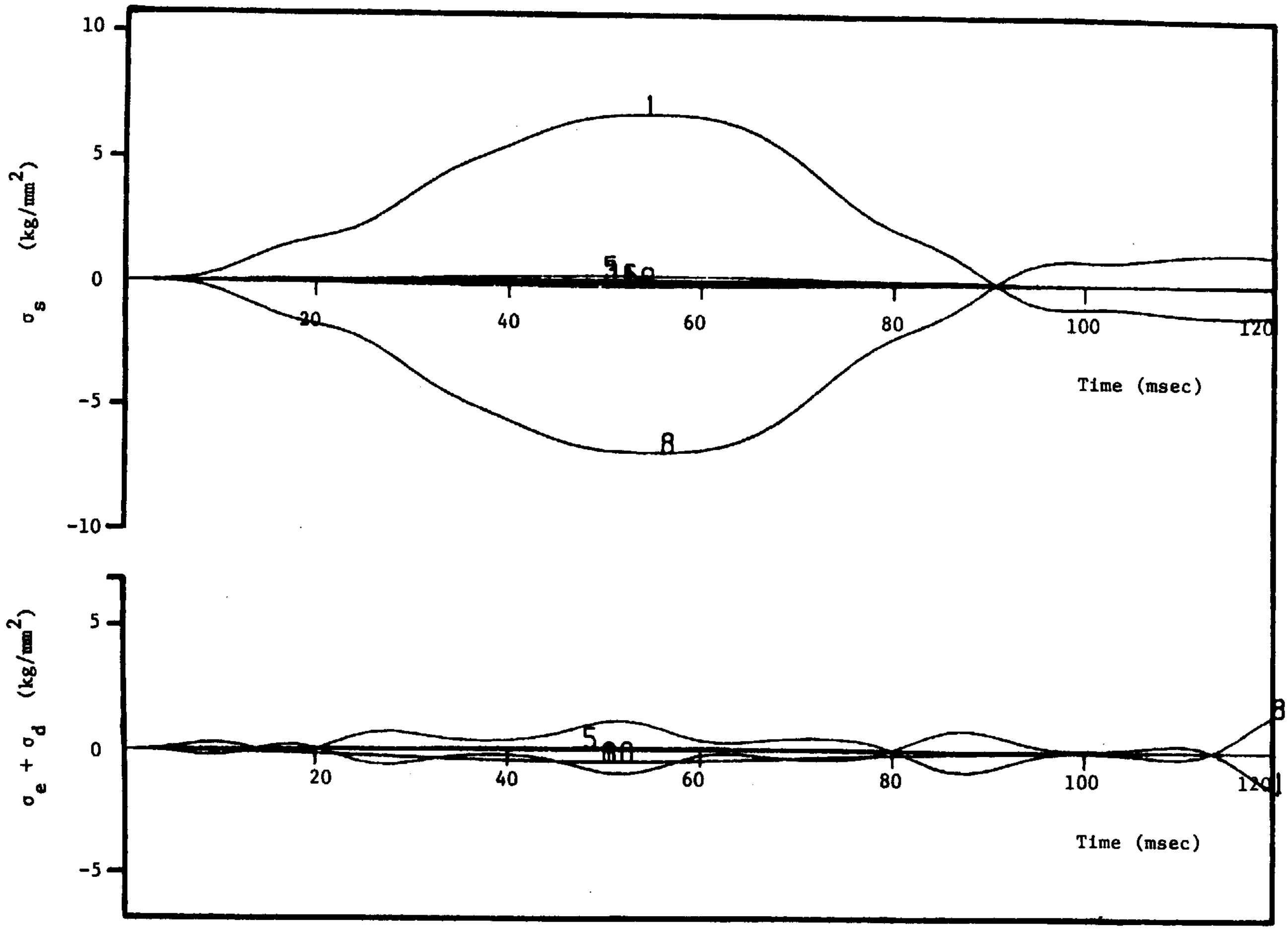

Fig.37 Time behaviors of σ_s and $\sigma_e + \sigma_d$ of the bellows for case 3 (element 26).

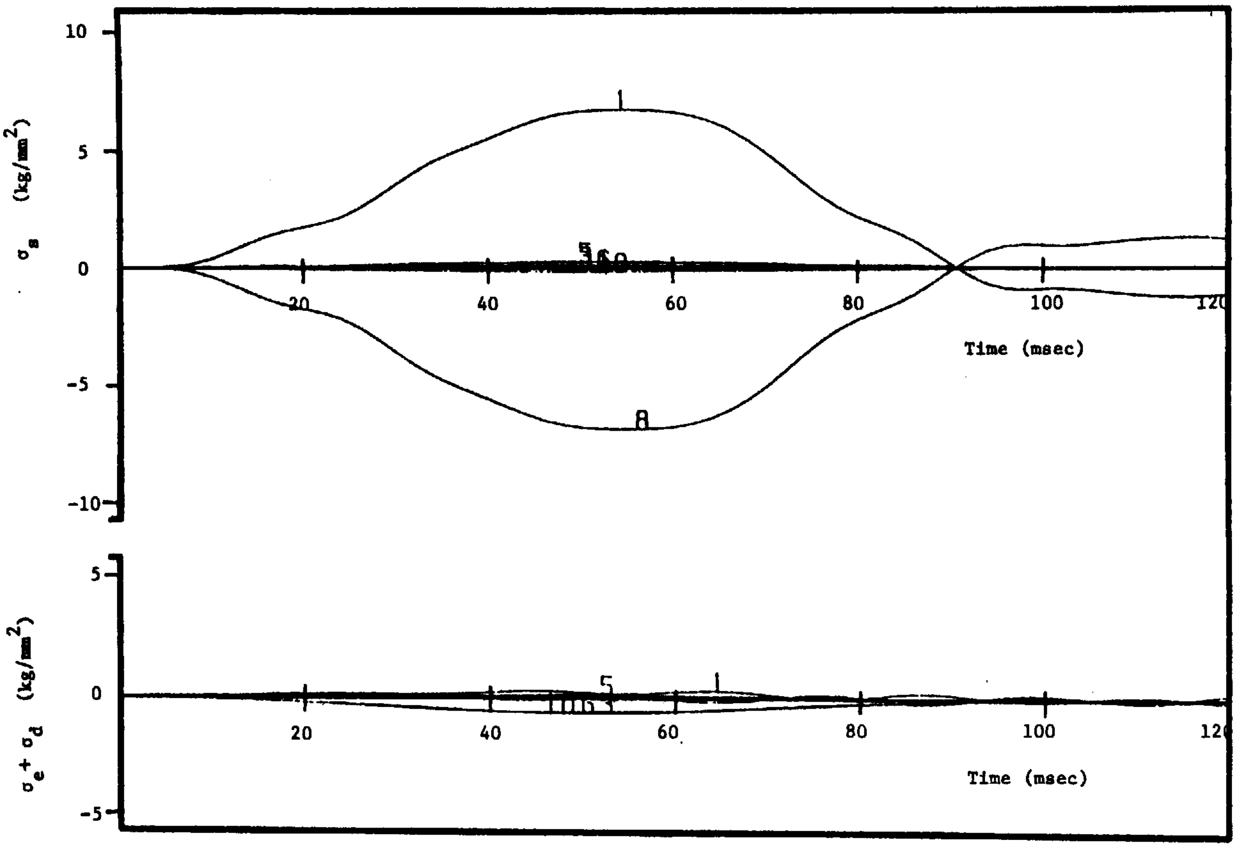

Fig.38 Time behaviors of σ_s and $\sigma_e+\sigma_d$ of the bellows for case 3 (element 122).

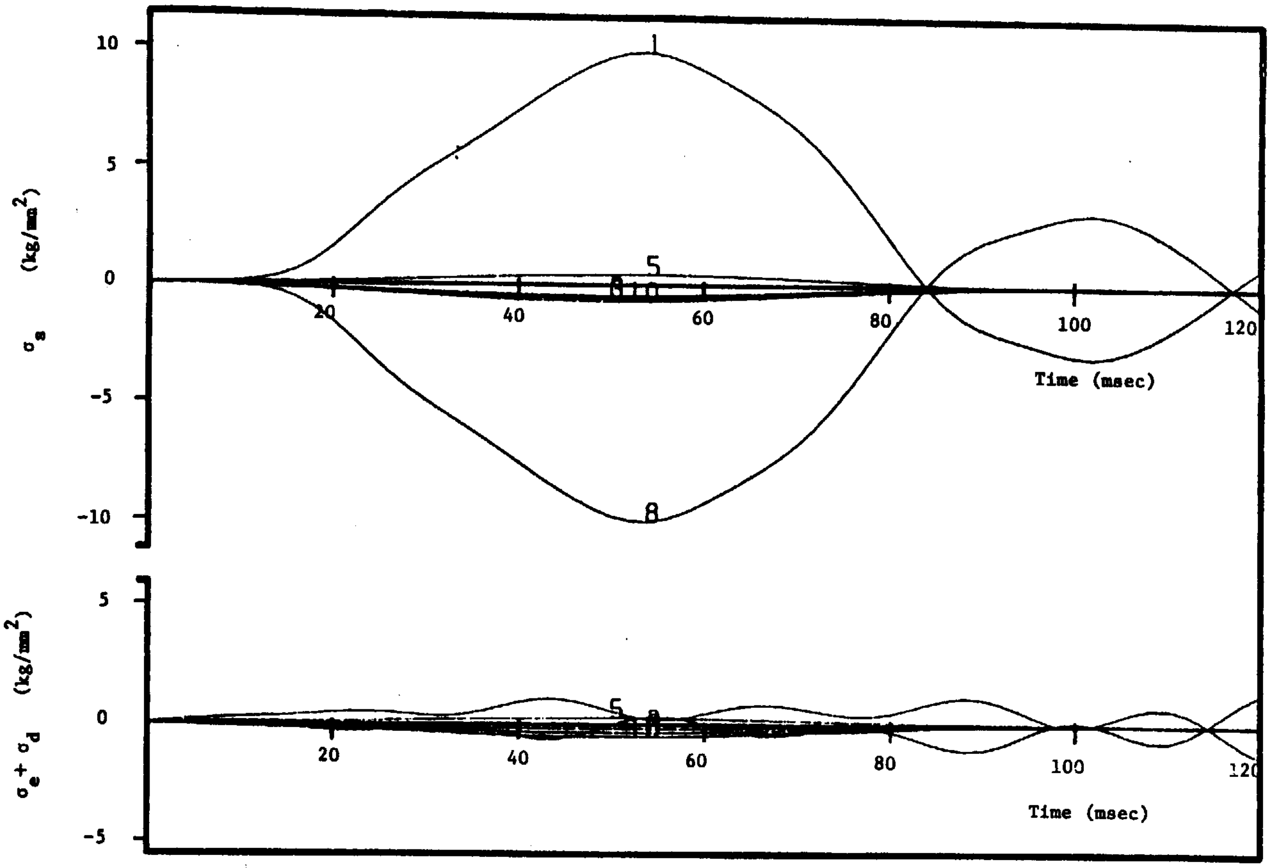

Fig.39 Time behaviors of σ_s and $\sigma_e+\sigma_d$ of the bellows for case 3 (element 31).

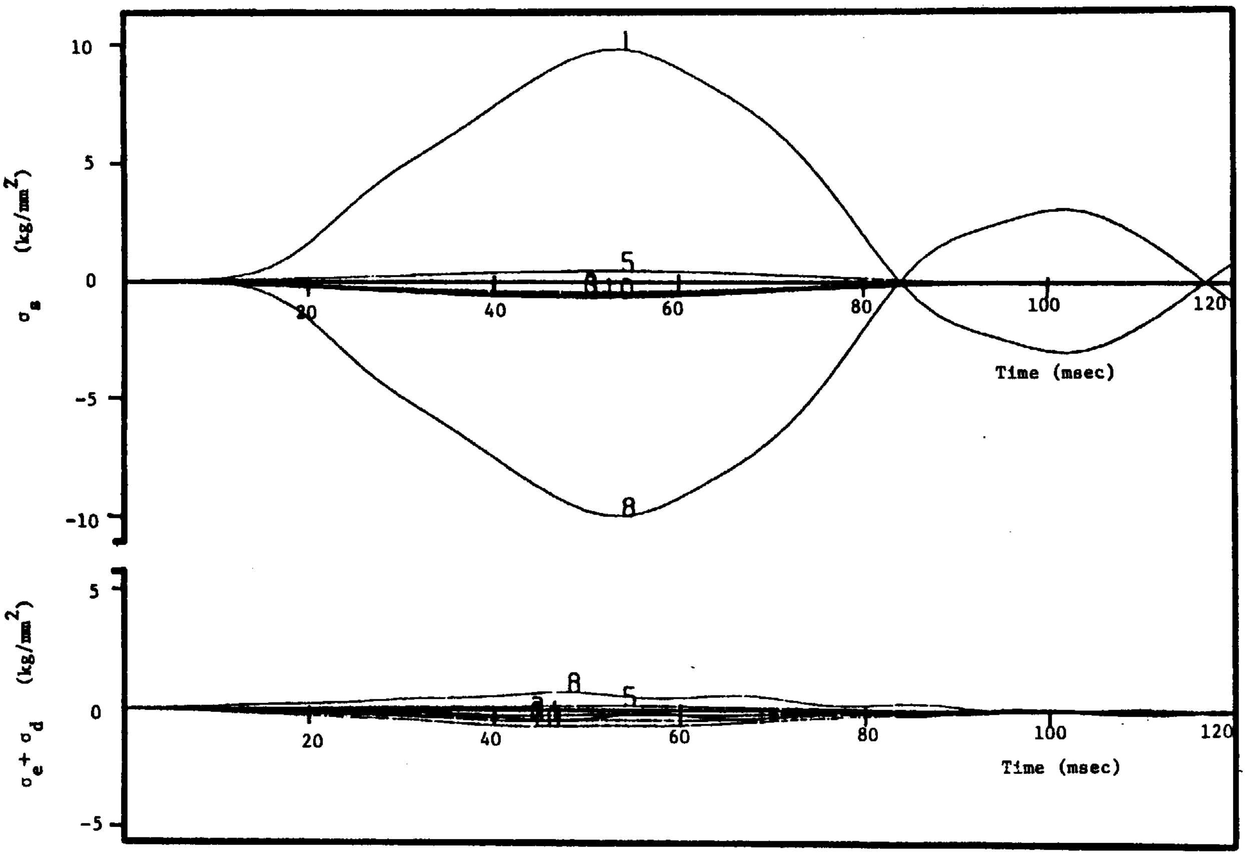

Fig.40 Time behaviors of σ_s and $\sigma_e + \sigma_d$ of the bellows for case 3 (element 127).

Table 1 Specifications of the overall and the bellows models.

Model	Overall	Bellows
Number of nodal points	390	196
Number of freedom	2154	928 before reduction 360 after reduction
Number of element		
Beam	123	52
Isotropic shell	316	24
Orthotropic shell	48	120

Table 2 Natural frequencies of the overall and the bellows models.

(a) Overall model

Mode	Freq.(Hz)	Mode	Freq.(Hz)	Mode	Freq.(Hz)	Mode	Freq.(Hz)
1	11.0	7	19.4	13	30.0	19	45.0
2	11.4	8	22.0	14	33.4	20	46.3
3	11.9	9	22.5	15	39.3	21	49.8
4	13.5	10	26.0	16	39.7	22	54.4
5	14.3	11	26.5	17	41.4	23	57.3
6	18.7	12	29.4	18	44.0	24	59.0

(b) Bellows model

Mode	Freq.(Hz)	Mode	Freq.(Hz)	Mode	Freq.(Hz)	Mode	Freq.(Hz)
1	15.7	4	36.6	7	44.3	10	47.3
2	29.0	5	38.7	8	44.7	11	49.7
3	29.3	6	43.9	9	46.2	12	51.9

Table 3 Load conditions for the dynamic response analysis.

Case	1	2	3
Plasma behavior	Plasma disruption with time constant of 1 msec	Plasma disruption with time constant of 50 msec	Start-up
Max. saddle-like eddy current (kA/m)	250	80	240
Max. inverse saddle-like eddy current (kA/m)	180	40	0
Number of repetition at R.T. at 400°C	 1000 0	 9000 1000	 45000 5000
Solution time step (msec)	1	2	2
Solution time duration (msec)	80	120	120

Table A1 γ_i at t = 3 msec in case 1.

I	γ_X	γ_Y	γ_Z
1	-0.119E+03	-0.383E+02	0.602E+03
2	-0.139E+02	-0.295E+01	0.439E+02
3	-0.116E+03	-0.467E+02	0.742E+03
4	-0.481E+02	0.624E+02	-0.111E+04
5	-0.207E+03	-0.591E+02	0.821E+03
6	0.495E+00	0.306E+02	-0.902E+03
7	0.364E+03	-0.381E+02	0.621E+03
8	0.524E+02	0.146E+03	-0.226E+04
9	-0.199E+03	-0.184E+02	0.276E+03
10	0.169E+03	-0.726E+01	0.257E+03
11	-0.518E+02	-0.561E+01	0.175E+03
12	-0.240E+03	0.703E+01	-0.178E+03
13	0.182E+02	0.341E+02	-0.133E+04
14	-0.403E+03	0.247E+03	-0.507E+04
15	-0.270E+04	-0.807E+02	-0.667E+04
16	0.501E+03	0.677E+02	0.101E+04
17	0.513E+02	-0.205E+02	0.429E+03
18	0.562E+03	-0.397E+03	0.940E+04
19	0.325E+03	-0.111E+03	0.259E+04
20	-0.136E+04	0.537E+03	-0.126E+05
21	-0.641E+02	0.165E+02	-0.444E+02
22	0.462E+04	0.503E+03	0.580E+04
23	-0.381E+03	0.269E+03	-0.511E+04
24	-0.153E+03	0.230E+02	-0.568E+03
25	-0.729E+01	-0.160E+02	0.529E+02
26	0.269E+03	-0.503E+02	0.221E+04
27	0.522E+04	0.231E+03	0.102E+05
28	0.139E+03	0.398E+02	0.731E+03
29	-0.224E+03	-0.325E+02	-0.497E+02
30	-0.458E+04	-0.109E+04	0.771E+04
31	-0.940E+03	-0.144E+03	-0.300E+04
32	-0.185E+03	-0.355E+02	-0.739E+03
33	-0.424E+02	-0.401E+01	-0.134E+03
34	-0.941E+02	-0.545E+01	0.437E+02
35	0.168E+03	-0.296E+02	0.592E+02
36	-0.982E+02	0.535E+02	-0.245E+01
37	0.256E+03	-0.373E+02	0.114E+03
38	-0.694E+03	-0.918E+02	0.158E+04
39	-0.376E+03	-0.815E+02	0.139E+04
40	-0.673E+02	-0.428E+02	0.195E+03
41	0.174E+04	0.511E+03	-0.420E+04
42	-0.763E+03	-0.547E+02	-0.371E+04
43	-0.956E+03	-0.131E+03	-0.410E+04

Table A2 γ_i at t = 16 msec in case 1.

I	γ_X	γ_Y	γ_Z
1	-0.265E+03	0.299E+02	-0.161E+04
2	-0.290E+02	0.244E+01	-0.125E+03
3	-0.267E+03	0.364E+02	-0.197E+04
4	0.570E+02	-0.289E+02	0.280E+04
5	-0.373E+03	0.659E+02	-0.254E+04
6	0.248E+03	0.113E+02	0.114E+04
7	0.674E+03	0.232E+02	-0.182E+04
8	0.521E+03	-0.125E+03	0.645E+04
9	-0.542E+03	0.125E+02	-0.817E+03
10	0.256E+03	-0.795E+01	-0.370E+03
11	-0.320E+03	-0.283E+02	-0.804E+03
12	-0.443E+03	0.116E+01	0.406E+03
13	0.442E+03	0.197E+02	0.137E+04
14	0.590E+02	-0.196E+03	0.112E+05
15	-0.480E+04	-0.722E+03	0.680E+04
16	0.120E+04	0.250E+03	0.213E+03
17	-0.294E+02	-0.571E+01	-0.854E+03
18	-0.111E+04	0.208E+03	-0.181E+05
19	-0.307E+02	0.514E+02	-0.571E+04
20	0.174E+02	-0.455E+03	0.263E+05
21	-0.202E+03	-0.129E+02	0.327E+03
22	0.109E+05	0.127E+04	-0.582E+04
23	0.136E+04	0.118E+03	0.835E+04
24	-0.107E+02	0.483E+02	0.636E+03
25	-0.114E+03	-0.287E+02	-0.752E+02
26	-0.296E+03	-0.478E+02	-0.178E+04
27	0.854E+04	0.609E+03	-0.660E+04
28	0.364E+03	0.136E+03	-0.412E+02
29	-0.676E+03	-0.863E+02	-0.181E+03
30	-0.168E+05	-0.105E+04	-0.194E+05
31	-0.782E+03	-0.711E+03	-0.196E+03
32	-0.125E+03	-0.218E+03	0.783E+03
33	-0.165E+03	-0.410E+02	-0.263E+02
34	-0.246E+03	-0.541E+02	0.209E+03
35	0.400E+02	-0.215E+03	0.367E+03
36	0.265E+03	0.356E+03	-0.141E+03
37	0.955E+02	-0.214E+03	-0.230E+03
38	-0.227E+04	-0.529E+03	0.170E+04
39	-0.182E+04	-0.394E+03	0.412E+03
40	-0.127E+03	-0.234E+03	-0.100E+04
41	0.495E+04	0.244E+04	0.751E+04
42	0.376E+04	-0.452E+03	-0.906E+04
43	0.647E+04	-0.108E+04	-0.143E+05

Table A3 γ_i at t = 10 msec in case 2.

I	γ_X	γ_Y	γ_Z
1	-0.392E+02	-0.106E+02	0.267E+03
2	-0.471E+01	-0.802E+00	0.201E+02
3	-0.371E+02	-0.129E+02	0.328E+03
4	-0.168E+02	0.186E+02	-0.446E+03
5	-0.617E+02	-0.150E+02	0.402E+03
6	0.134E+02	0.109E+02	-0.306E+03
7	0.137E+03	-0.109E+02	0.257E+03
8	0.158E+02	0.356E+02	-0.979E+03
9	-0.786E+02	-0.386E+01	0.109E+03
10	0.568E+02	-0.325E+01	0.773E+02
11	-0.361E+02	-0.434E+01	0.106E+02
12	-0.866E+02	0.270E+01	-0.593E+02
13	0.316E+02	0.145E+02	-0.437E+03
14	-0.161E+03	0.732E+02	-0.211E+04
15	-0.870E+03	0.228E+02	-0.250E+04
16	0.166E+03	0.904E+01	0.427E+03
17	0.156E+02	-0.640E+01	0.157E+03
18	0.176E+03	-0.123E+03	0.374E+04
19	0.104E+03	-0.359E+02	0.101E+04
20	-0.492E+03	0.164E+03	-0.521E+04
21	-0.450E+02	0.217E+01	-0.587E+02
22	0.136E+04	0.529E+02	0.220E+04
23	-0.165E+03	0.750E+02	-0.197E+04
24	-0.493E+02	0.874E+01	-0.179E+03
25	0.368E+01	-0.284E+01	0.129E+02
26	0.765E+02	-0.221E+02	0.767E+03
27	0.170E+04	-0.268E+02	0.370E+04
28	0.429E+02	0.450E+01	0.345E+03
29	-0.615E+02	-0.587E+01	-0.701E+02
30	-0.141E+04	-0.190E+03	0.295E+04
31	-0.446E+03	-0.587E+02	-0.114E+04
32	-0.731E+02	-0.156E+02	-0.303E+03
33	-0.292E+02	-0.856E+00	-0.124E+03
34	-0.461E+02	-0.328E+01	-0.223E+02
35	0.482E+02	-0.131E+02	-0.118E+03
36	0.440E+02	0.220E+02	0.345E+03
37	0.462E+02	-0.136E+02	-0.200E+03
38	-0.368E+03	-0.405E+02	0.140E+03
39	-0.239E+03	-0.294E+02	0.335E+02
40	-0.891E+02	-0.233E+02	-0.338E+02
41	0.153E+04	0.258E+03	0.289E+03
42	-0.931E+03	-0.109E+03	-0.134E+04
43	-0.166E+04	-0.219E+03	-0.229E+04

Table A4 γ_i at $t = 52$ msec in case 2.

I	γ_X	γ_Y	γ_Z
1	-0.106E+03	0.162E+02	-0.425E+03
2	-0.117E+02	0.133E+01	-0.330E+02
3	-0.105E+03	0.197E+02	-0.520E+03
4	0.171E+02	-0.167E+02	0.761E+03
5	-0.144E+03	0.346E+02	-0.668E+03
6	0.107E+03	0.451E+01	0.268E+03
7	0.290E+03	0.128E+02	-0.506E+03
8	0.178E+03	-0.696E+02	0.172E+04
9	-0.222E+03	0.786E+01	-0.222E+03
10	0.105E+03	-0.418E+01	-0.102E+03
11	-0.145E+03	-0.145E+02	-0.292E+03
12	-0.186E+03	0.905E+00	0.118E+03
13	0.202E+03	0.117E+02	0.311E+03
14	0.337E+01	-0.912E+02	0.294E+04
15	-0.148E+04	-0.164E+03	0.162E+04
16	0.343E+03	0.626E+02	0.167E+03
17	-0.737E+01	-0.912E+00	-0.228E+03
18	-0.451E+03	0.955E+02	-0.468E+04
19	-0.180E+02	0.217E+02	-0.155E+04
20	0.119E+02	-0.194E+03	0.688E+04
21	-0.107E+03	-0.101E+02	0.754E+02
22	0.333E+04	0.277E+03	-0.135E+04
23	0.397E+03	0.266E+02	0.213E+04
24	-0.149E+02	0.199E+02	0.166E+03
25	-0.188E+02	-0.689E+01	-0.200E+02
26	-0.137E+03	-0.297E+02	-0.372E+03
27	0.273E+04	0.254E+02	-0.139E+04
28	0.612E+02	0.330E+02	0.887E+02
29	-0.224E+03	-0.228E+02	-0.775E+02
30	-0.544E+04	-0.131E+03	-0.517E+04
31	-0.332E+03	-0.220E+03	-0.200E+03
32	-0.306E+02	-0.722E+02	0.191E+03
33	-0.583E+02	-0.135E+02	-0.545E+02
34	-0.102E+03	-0.203E+02	0.664E+02
35	0.588E+02	-0.795E+02	0.506E+02
36	0.751E+02	0.126E+03	0.610E+02
37	0.839E+02	-0.759E+02	-0.153E+03
38	-0.914E+03	-0.193E+03	0.664E+03
39	-0.689E+03	-0.141E+03	0.164E+03
40	-0.959E+02	-0.840E+02	-0.289E+03
41	0.252E+04	0.862E+03	0.201E+04
42	0.499E+03	-0.159E+03	-0.263E+04
43	0.747E+03	-0.403E+03	-0.416E+04

Table A5 γ_i at $t = 50$ msec in case 3.

I	γ_X	γ_Y	γ_Z
1	-0.266E+03	0.340E+02	-0.171E+04
2	-0.291E+02	0.276E+01	-0.132E+03
3	-0.265E+03	0.413E+02	-0.209E+04
4	0.625E+02	-0.348E+02	0.298E+04
5	-0.371E+03	0.730E+02	-0.268E+04
6	0.257E+03	0.947E+01	0.124E+04
7	0.672E+03	0.270E+02	-0.193E+04
8	0.535E+03	-0.141E+03	0.683E+04
9	-0.549E+03	0.144E+02	-0.865E+03
10	0.253E+03	-0.772E+01	-0.402E+03
11	-0.328E+03	-0.290E+02	-0.846E+03
12	-0.442E+03	0.687E+00	0.433E+03
13	0.457E+03	0.179E+02	0.151E+04
14	0.909E+02	-0.222E+03	0.119E+05
15	-0.476E+04	-0.739E+03	0.752E+04
16	0.120E+04	0.254E+03	0.148E+03
17	-0.342E+02	-0.435E+01	-0.914E+03
18	-0.119E+04	0.246E+03	-0.194E+05
19	-0.563E+02	0.616E+02	-0.609E+04
20	0.120E+03	-0.513E+03	0.281E+05
21	-0.293E+03	-0.147E+02	0.342E+03
22	0.110E+05	0.127E+04	-0.644E+04
23	0.144E+04	0.102E+03	0.901E+04
24	0.104E+00	0.484E+02	0.699E+03
25	-0.117E+03	-0.285E+02	-0.816E+02
26	-0.328E+03	-0.461E+02	-0.201E+04
27	0.644E+04	0.609E+03	-0.758E+04
28	0.365E+03	0.138E+03	-0.951E+02
29	-0.683E+03	-0.867E+02	-0.184E+03
30	-0.171E+05	-0.998E+03	-0.206E+05
31	-0.740E+03	-0.725E+03	0.183E+02
32	-0.115E+03	-0.223E+03	0.865E+03
33	-0.168E+03	-0.421E+02	-0.181E+02
34	-0.248E+03	-0.557E+02	0.213E+03
35	0.302E+02	-0.221E+03	0.374E+03
36	0.301E+03	0.364E+03	-0.145E+03
37	0.844E+02	-0.219E+03	-0.247E+03
38	-0.230E+04	-0.542E+03	0.164E+04
39	-0.155E+04	-0.402E+03	0.325E+03
40	-0.127E+03	-0.239E+03	-0.105E+04
41	0.501E+04	0.248E+04	0.807E+04
42	0.393E+04	-0.464E+03	-0.909E+04
43	0.673E+04	-0.111E+04	-0.144E+05